Nonlinear Transient Analysis of Piezoelectric FGM Plate Under Electro-Thermo-Mechanical Loading

An
M.Tech Dissertation Report

By
Saurav Sharma

(2015PDE5111)

DEPARTMENT OF MECHANICAL ENGINEERING
MALAVIYA NATIONAL INSTITUE OF TECHNOLOGY,
JAIPUR, RAJASTHAN

June 2017

A

Dissertation Report

on

Nonlinear Transient Analysis of Piezoelectric FGM Plate Under Electro-Thermo-Mechanical Loading

Submitted in the Partial Fulfillment of the Requirement for the Degree of

Master of Technology
in
Design Engineering

By
Saurav Sharma
(2015PDE5111)

Under the Supervision of

Dr. Dinesh Kumar

DEPARTMENT OF MECHANICAL ENGINEERING
MALAVIYA NATIONAL INSTITUTE OF TECHNOLOGY
JAIPUR-302017 (RAJASTHAN)

June 2017

DEPARTMENT OF MECHANICAL ENGINEERING
MALAVIYA NATIONAL INSTITUTE OF TECHNOLOGY
JAIPUR (RAJASTHAN)-302017

CERTIFICATE

This is to certify that the dissertation work entitled **"Nonlinear Transient Analysis of Piezoelectric FGM Plate Under Electro-Thermo-Mechanical Loading"** by Mr. Saurav Sharma (ID.No. 2015PE5111) is a bonafide record of independent research work completed under my supervision and guidance, and hence approved for submission to the Department of Mechanical Engineering, Malaviya National Institute of Technology in partial fulfillment of the requirements for the award of the degree of Master of Technology with specialization in Design Engineering. The matter embodied in this report has not been submitted for the award of any other degree, or diploma to any other institute/university.

Date: / /
Place: Jaipur

Dr. Dinesh Kumar
Assistant Professor,
Mechanical Engineering Department,
MNIT, Jaipur (Raj.)

DEPARTMENT OF MECHANICAL ENGINEERING
MALAVIYA NATIONAL INSTITUTE OF TECHNOLOGY
JAIPUR (RAJASTHAN)-302017

DECLARATION

I, **Saurav Sharma** (ID-2015PDE5111) hereby declare that the dissertation entitled **"Nonlinear Transient Analysis of Piezoelectric FGM Plate Under Electro-Thermo-Mechanical Loading"** being submitted by me in the partial fulfillment of the requirements for the award of the degree of **M. Tech (Design Engineering)** is a research work carried out by me under the supervision of **Dr. Dinesh Kumar,** and that the contents of this dissertation work, in full or in parts, have not been submitted to any other Institute or University for the award of any degree or diploma. I also certify that no part of this dissertation work has been copied or borrowed from anyone else. In case any type of plagiarism is found out, I will be solely and entirely responsible for it.

Date: / /

Place: Jaipur

Saurav Sharma
M.Tech. (Design Engineering)
2015PDE5111

ACKNOWLEDGEMENT

I feel immense pleasure in conveying my heartiest thanks and profound gratitude to my supervisor **Dr. Dinesh Kumar,** who provided me with his generous guidance, valuable help, and endless encouragement by taking personal interest and attention. No words can fully convey my feelings of respect and regard for him. Also, I would like to thank **Mr. Kanishk Sharma,** Ph.D. Scholar, Department of Mechanical Engineering, MNIT, Jaipur, for his invaluable support in carrying out this research work. He has helped me in understanding the core concepts of plate theory and developing the code, without which the completion of this thesis would not have been possible.

I also express my deepest gratitude to my **parents** for their blessings, affection, and belief, which inspired me to carry on my work through hard times. Last, but not the least I thank one and all who have helped me directly or indirectly in the completion of the report.

ABSTRACT

This thesis is aimed at studying the nonlinear static and transient responses of FGM and smart FGM plates. The smart FGM plate consists of an FGM layer bonded with thin piezoelectric actuator layers on top and bottom surfaces. The volume fractions of FGM constituents (ceramic and metal) are varied according to simple power law distribution in the thickness direction. The FGM layer is modeled as a single layer of inhomogeneous material with continuously varying properties, with Poison's ratio kept constant. The steady state responses of an FGM plate and smart FGM plate are calculated for suddenly applied uniform lateral pressure and thermo-electro-mechanical load respectively. Furthermore, the dynamic analysis is also performed to calculate the transient responses of both the FGM and smart FGM plates.

A finite element formulation based on first-order shear deformation plate theory is developed, to include the geometric nonlinearities in the von-Karman sense. An incremental solution technique based on Newton-Raphson iterative scheme is applied to solve the nonlinear algebraic equations, obtained using FEM formulation. Newmark-Beta Integration Scheme is applied to approximate the time derivatives in dynamic analysis of smart FGM plate, and the nonlinear transient response is computed using incremental solution technique. An uncoupled ESL (Equivalent Single Layer) model is used to account for the mechanical contributions of the piezoelectric layer due to the applied actuator voltage.

The accuracy of present formulation is verified by comparing the results with the relevant literature, and parametric studies are performed to investigate the effects of various material, geometrical, and loading parameters on nonlinear steady-state and transient responses of both FGM and smart FGM plates with different boundary conditions.

It is revealed that the application of a positive voltage on smart FGM plate increases the transverse deflections, whereas the transverse deflections are suppressed due to the negative voltage. The temporal variation of smart FGM plate is not affected significantly by the applied voltage for initial time steps, but as the time progresses the effect of applied voltage increases rapidly, i.e., there is a time lag between the application of load and the beginning of actuation.

Contents

List of Figures

List of Tables

List of Abbreviations

FGM	Functionally graded material
a	Length of FGM plate
b	Width of FGM plate
h	Thickness of FGM plate
h_a	Thickness of Piezoelectric Layer
n	Power law index
E	Young's modulus
E_c	Young's modulus of ceramic constituent
E_m	Young's modulus of metal constituent
E_p	Young's modulus of piezoelectric material
V_c	Volume fraction of ceramic constituent
V_m	Volume fraction of metal constituent
Al	Aluminum
Al_2O_3	Alumina
ν	Poisson's ratio
W_{max}	Maximum transverse deflection
W	Normalized maximum transverse deflection
N_{xx}, N_{xy}, N_{yy}	Force resultants per unit area
M_{xx}, M_{xy}, M_{yy}	Moment resultants per unit area
u, v & w	Displacements along x, y & z directions
u_0 , v_0 & w_0	Mid-plane displacements along x, y & z directions
$\varepsilon_{xx}, \varepsilon_{yy}, \varepsilon_{zz}$	Linear strains
$\gamma_{yz}, \gamma_{xz}, \gamma_{xy}$	Shear strains
$\sigma_{xx}, \sigma_{yy}, \sigma_{zz}$	Axial stresses

$\sigma_{xy}, \sigma_{yz}, \sigma_{zx}$	Shear stresses
V	Voltage

Chapter 1

INTRODUCTION

1.1. The Functionally Graded Materials (FGM)

FGMs are the new kind of composite materials containing nonhomogeneous properties and are made of different material constituents, usually ceramics and metals. They possess a smooth and continuous/stepwise variation of properties obtained by varying the volume fractions of their constituents in any directions, usually in thickness direction, to design a material for some specific applications, especially high temperature.

There are two possible ways of variation of properties to form a composite material, continuous variation, and stepwise variation. If varied continuously, the transition of properties from one point to the next in the thickness direction is smooth, as in FGMs. On the other hand, if the stepwise variation is used, there forms a layered structure, resulting in abrupt transition of properties, leading to high thermal and structural stresses [1], as in conventional laminated composites. These two arrangements are depicted in Fig. (1).

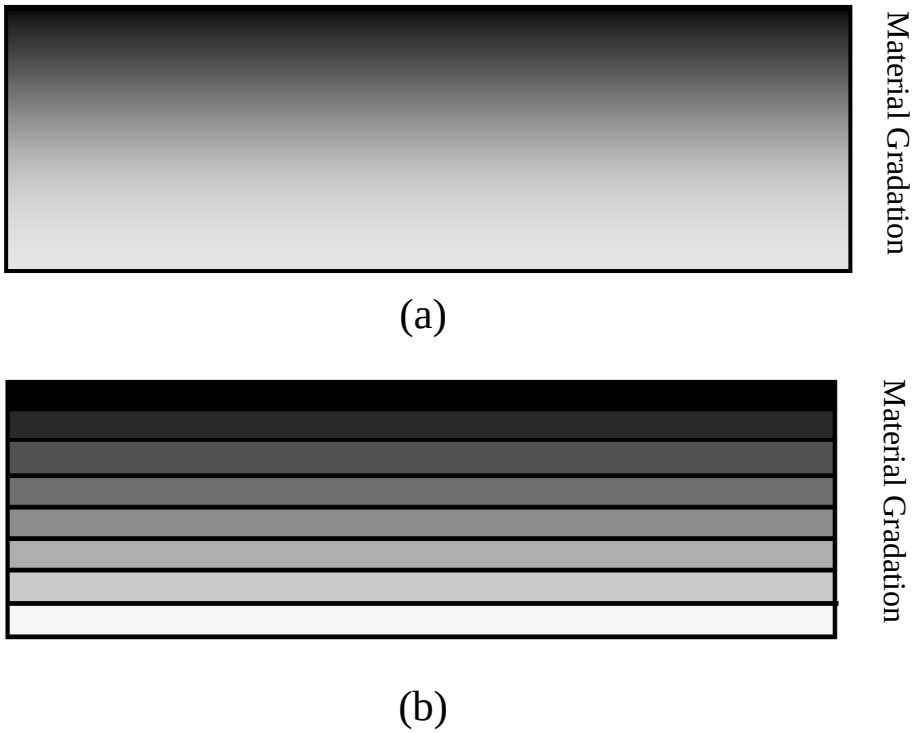

Fig. 1. FGM with (a) continuous gradation, and (b) stepwise gradation.

1.1.1. Background and Motivation

With the evolvement of science and technology, the fields of engineering have expanded to areas where machines and their components are required to withstand highly adverse working and environmental conditions. Homogeneous materials with single constituent find very less application in such conditions, which calls for the development of new advanced materials, like, composites and nanomaterials. One such advancement is the development of Functionally Graded Materials (FGM).

The concept of FGM was initially introduced to serve the purpose of heat shield for the space reentry vehicles. During reentry into the earth's atmosphere, a spacecraft traveling at hypersonic speeds develops aerodynamic heating, which in turn can damage/destroy the spacecraft, if no protection system is used. The commonly used protection systems, such as ablators, tiles, and blankets, absorb heat and get consumed during reentry. These shields are structurally weak and get damaged easily, and that was the main cause of space shuttle Columbia disaster[2]. Thus, the inclusion of metal, to provide sufficient strength and toughness to the material, into a Thermal Protection system (TPS) was felt. However, abrupt change of material composition and properties, as in the case of conventional laminated composites, results in stress concentration, and hence, not suitable for TPS. Hence, by employing FGMs, we utilize the desirable properties of both metal and ceramic, without worrying about the stress concentration issue caused by the creation of interfaces.

The first practical use of FGM was reported in 1984 at National Aerospace Laboratories of Japan [3] The combination of materials (i.e., metal and ceramic) was used to sustain a temperature of 2000 K with a temperature gradient of 1000 K across 10 mm distance. Nowadays, in the steam power plant, the turbine blades under high-temperature conditions may be made as a mixture of ceramic and metal, having metal on the low-temperature side and ceramic on the high-temperature side with a gradual variation of composition in between, to provide a smooth transition of material properties[4].

1.1.2. Types of FGM

Due to the wide scope of applications of FGMs, there are various types of FGMs developed over the time. Based on the types of applications, different types of gradation, naturally or man-made have been seen/employed in FGMs. For instance, most of the human body parts have natural graded composition. Thus, the implants also need to be

made in graded fashion to mimic the organ they are intended to replace. The FGMs are divided into three categories namely, chemical composition gradient FGM, porosity gradient FGM and the microstructural gradient FGM [5].

Chemical composition gradient FGMs are engineered so as to have varying chemical composition gradually with varying spatial coordinates. This can be done in both single phase or multiphase material. Single phase FGM is produced due to the solubility of one phase into another. The phase diagram suggests that some materials when mixed with others tend to dissolve and make a single-phase material. The gradation of properties occurs due to varying solubility. However, this type of FGM is less common. The other type of chemical composition gradient FGMs, which are more common, are multi-phased chemical composition gradient materials. Here, the chemical composition is varied through the bulk volume of the FGM from one material to the other. The variation in properties is controlled by controlling the proportion of constituents and its variation, according to the requirement of the intended application.

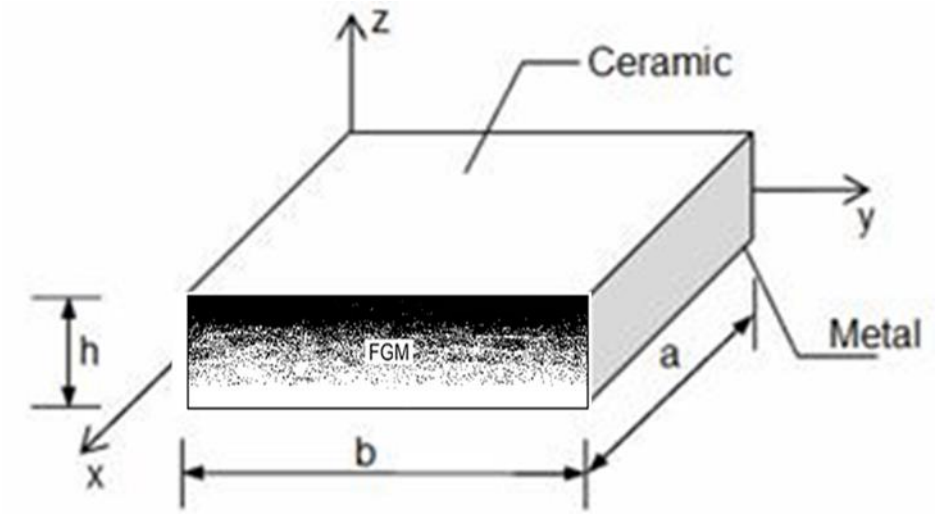

Fig. 2. Schematic of a metal-ceramic functionally graded plate.

It is well known that not only the constituents of a material, but also the inner porosities and their spatial positions have influence on its properties. **The porosity gradient FGMs** are the materials in which the porosity of the material is varied with the space coordinates of the bulk material. The shape, size, and density of the pores are the deciding factors in governing the material properties according to the intended application, for which the FGM is being manufactured. This type of FGMs find their use in human body implants, especially the bone implants for providing support to the

bone growth. The gradual change in pore density helps absorbing the shocks, provides thermal insulation. In actual, the real bones are **porosity gradient FGMs** having graded porosity, which aids in healing and blood circulation. Due to these reasons porosity FGMs have widespread applications in the biomedical field.

Microstructure graded FGMs are the type of FGM in which microstructure is tailored so as to produce different microstructures in the material. The smooth gradation in microstructure gives smoothly varying properties in the material, eliminating stress concentrations and sharp interfaces. This type of varying microstructure is generated during the solidification process. For example, manufacturing a component with high toughness and hard surface can be done by cooling the inner core slowly and allowing the outer surface to cool rapidly. This produces graded microstructure from inner to outermost part of the material. Another way to achieve graded microstructure is by using controlled heat treatment process. The gradation of the microstructure to manufacture an FGM is shown in Fig. 3.

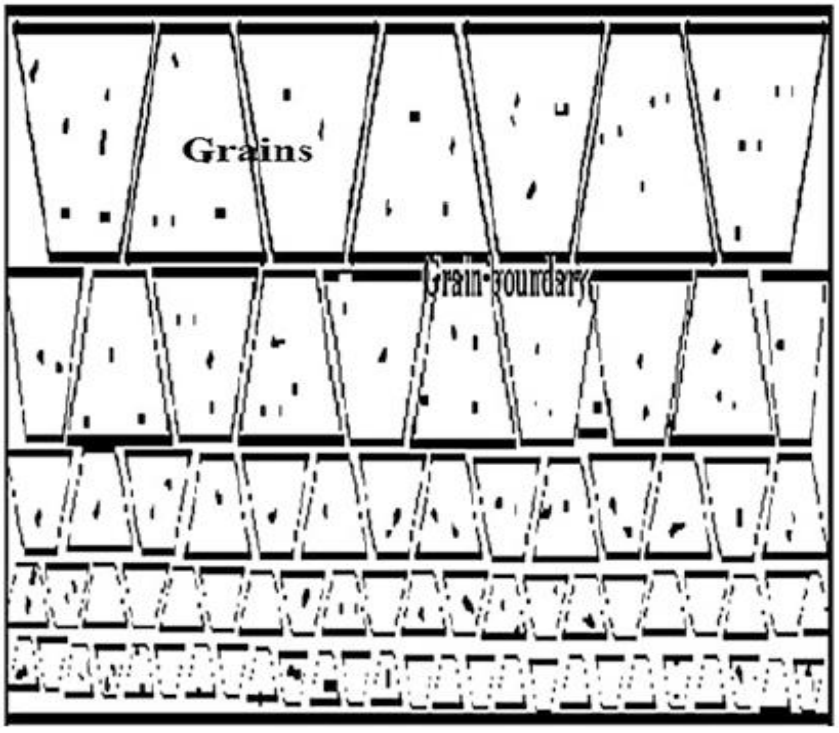

Fig. 3. Schematic of a graded microstructure FGM [5].

In addition to the above, structural elements, such as, plates, shells, etc., made of smart FGMs are also one of the new emerging advancements in the field of composite structures. The idea behind an adaptive or smart FGMs is to have a continuous check

on their condition during the function and also to control their response, to increase their reliability. The smart FGM plates are made by employing one or more layers of piezoelectric materials on the FGM plate. This thesis is focused on exploring the behavior of a smart FGM plate under electro-thermo-mechanical conditions by developing a mathematical model and to perform various parametric studies.

1.2. Smart or Adaptive FGM Structures

With the increasing demand of reliability and accuracy of structures, a new concept of advanced materials being used nowadays is to monitor and control the behavior of the structures by bonding actuators and sensors to the material. The structures employing these materials promote high performance and reliability and are termed as smart or adaptive structures [6]. A smart structure has following two functions, besides providing structural integrity:

i. Sensing, which includes sending electric signals corresponding to structure's response, and
ii. Actuation, which is the response that it generates in the material corresponding to the received electric signal.

Use of these structures becomes essential in the locations where actuation and sensing are critical for avoiding any hazardous situation, that may arise due to uncontrolled vibrations or deflections. Also, the real-time control of structure helps monitor the health of a structure for increased life and proper working during service.

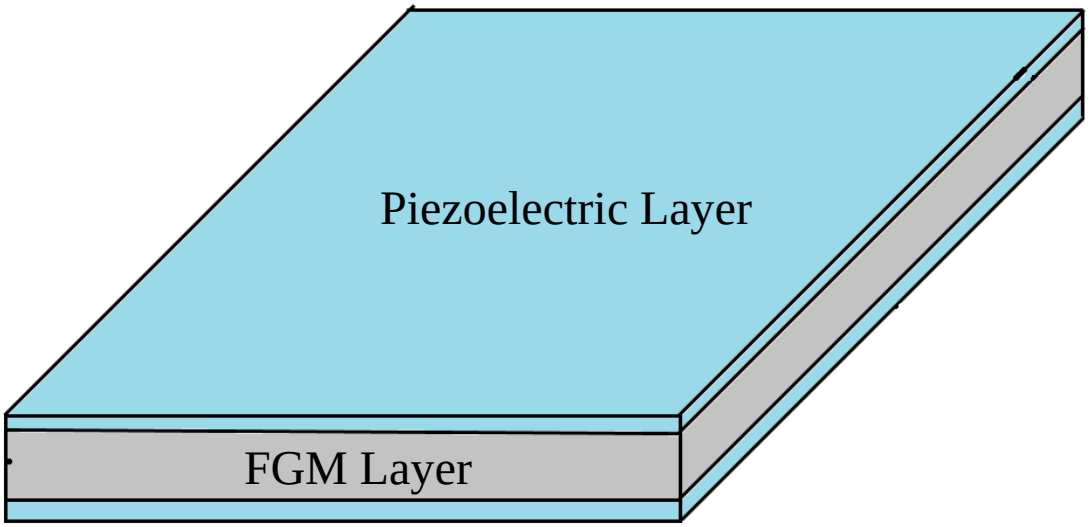

Fig. 4. Rectangular FGM plate sandwiched between two piezoelectric layers.

Use of FGMs with actuator layers, as shown in Fig. 4, has found its scope in almost every possible area of applications, where FGMs are already being used. The reason behind the extensive use of these smart structures is the benefits [7] that it offers over the conventional composites. Following are the main advantages of adaptive FGMs:

- It provides opportunities to take the benefits (pros) of different material properties (i.e., resistance to oxidation, machinability, toughness, and bonding capability).
- It provides multi-functionality.
- It provides the ability to control deformation, corrosion, wears, dynamic response and ability to design for different complex environments.
- It provides the ability to remove stress concentrations.
- Due to actuation characteristics, it facilitates with the real-time monitoring and controlling of the structures where a high level of accuracy must be maintained.

Following are the few areas, where adaptive or smart structures are being used extensively [6]:

- Process Monitoring
- Vibration isolation and control
- Biomedical

- Micro-electro-mechanical devices
- Aerospace applications

Besides aforementioned advantages and broad area of application, smart FGMs are also faced with some challenges/limitations, as follows, which may limit their use for some applications.

- Due to continuous variation of properties in one or multiple directions, the modelling of these materials becomes challenging.
- Computer simulations of materials under various working and environmental conditions would require high computation time and cost if the materials are nonhomogeneous with properties being functions of space coordinates and especially, when the sensor and actuator layers are also considered in the formulation.
- When the electric field applied in the direction of poling is more than the dielectric strength of the piezoelectric layer, an electric breakdown may happen [8]. This electric breakdown may destroy the piezoelectric properties of the material. This limits the amount of applied electric field, which in turn limits the amount of actuation that can be employed during service.

1.3. Objectives of the Thesis

This thesis is aimed at achieving the following research objectives:

- to investigate steady state (i.e., static) nonlinear response of an FGM plate under suddenly applied lateral uniform pressure,
- to analyze steady state response of the FGM plate bonded with piezoelectric actuator layers (i.e., smart FGM plate) under electro-thermo-mechanical loading,
- to study nonlinear transient response of the FGM plate under an impact load,
- to examine the nonlinear transient response of the smart FGM plate, subjected to electro-thermo-mechanical loading, and
- to carry out parametric studies to investigate the effects of geometric, material, and loading parameters on the nonlinear steady state and transient responses of the FGM and smart FGM plates, under different boundary conditions.

1.4. Outline of the Thesis

- Chapter 1 introduces the concept of functionally graded material and adaptive structures, their types, applications, and advantages and in the end, the objectives of the thesis are outlined.
- Chapter 2 deals with a comprehensive review of the past research done on FGM and adaptive FGM structures under various geometric, material, and loading conditions. Based on this review, research gaps are identified, and the problem statement is envisioned.
- Chapter 3 provides the mathematical formulation for solving the problem on FGM and smart FGM plates under electrical and/or thermal and/or mechanical loads. Mindlin's first order shear deformation theory based finite element formulation is developed. The constitutive relations used in considering the piezoelectric and thermal effects are provided. Newmark integration scheme, Newton-Raphson iterative scheme, and different boundary conditions are also explained. At last, a schematic in the form of a flow chart is given to show the stepwise methodology to carry out the nonlinear dynamic analysis.
- Chapter 4 contains the results and discussions for the static and dynamic analyses of FGM and smart FGM plates. The parametric studies are also conducted to investigate the effects of various parameter, viz. the volume fraction of FGM constituents, the slenderness ratio, the ratio of thicknesses of FGM and piezoelectric layers, and the applied actuator voltage on responses of FGM or smart FGM plates. Controlling effect of actuator voltage on the nonlinear response of the plate structure is also shown.
- The key conclusions drawn from the present study are given in the Chapter 5, along with the future scope in this area of research.

Chapter 2

LITERATURE REVIEW

In this chapter, a comprehensive survey of the state-of-art research work related to analysis of FGM and piezoelectric FGM plates is presented. After a brief review of the literature related to homogeneous plates in the beginning, the studies related to FGM plates and their behavior under thermal and/or mechanical loads are reviewed. The past works carried out by many researchers in the field of piezoelectric FGM plates are also reviewed, before highlighting the research gaps in the end of this chapter.

The idea of a material with graded properties was first introduced by Shen and Bever [8-9] in 1972. After that, different types of models and their applications have been proposed by many researchers for grading composition, filament concentration, polymerization, over the years [7]. It was in 1984 that the FGM was utilized for the first time in a practical application in space reentry vehicles as Thermal Protection Systems (TPS) at the National Aerospace Laboratories of Japan [3].

The plate and shell structures widely used in engineering applications are prone to failure due to excessive lateral deflections or stresses. Therefore, it becomes critical to evaluate and analyze the deflections of such structures, including the nonlinear effects. One of the very first attempts of this kind was made by Akay [11] for homogeneous, isotropic plates. Later, the work of Akay was extended by Reddy [12-13] for the nonlinear transient response of isotropic and orthotropic laminated plates based on Reissner and Mindlin's plate theory and Newmark time integration scheme.

Praveen and Reddy [14] investigated the large deformations of rectangular plates under thermomechanical loads. Results for both static and transient responses of FGM plates were presented for different boundary conditions and volume fractions of constituents. Moderately large deformations have been computed in von Karman sense, and time approximations of the deflection were based on Newmark integration scheme. Later on, Reddy and Chin [15] developed a procedure for the analysis of large defections of FGM plates and cylinders using finite element model, including the thermomechanical couplings in the formulation. Further, the formulations based on third-order shear deformation theory and Navier's solution were reported by Reddy [16] for the nonlinear transient analysis of metal-ceramic FGM plates, under thermomechanical loading. Properties of FGM were varied according to a power law in all the studies of Reddy.

Furthermore, the static large deflections of an FGM shell were analyzed by Woo and Meguid [17]. Yang and Shen [18] reported the transient response of FGM plates subjected to transverse mechanical loads along with their vibration characteristics. Reddy's higher order theory based formulation was used in the study and properties of the constituents are distributed across the thickness according to a power law in terms of the volume fractions of the constituent materials. In another study of Yang and Shen [19], a transverse mechanical load was applied under the influence of a temperature field to investigate the effects of load parameter, material properties, and shell geometry.

Qian et al. [20] reported the static and dynamic deformations of a thick rectangular functionally graded plate, made of two isotropic constituents and whose effective properties are computed by using Mori-Tanaka homogenization technique. A higher-order shear and normal deformable plate theory (HOSNDPT) implemented through meshless local Petrov-Galerkin (MLPG) method was employed in the analysis of FGM plates by Qian et al [20].Shen [21] performed the nonlinear bending analysis of a simply-supported FGM plate subjected to uniform and sinusoidal transverse loads. Use of mixed Galerkin-perturbation technique was made to get the load-deflection and load-bending moment curves. In another analysis, Qian and Batra [22] used meshless local Petrov-Galerkin (MLPG) method to compute the transient response of a thick functionally graded plate based on higher-order shear and normal deformable plate theory (HOSNDPT) when subjected to a heat flux and transverse mechanical load. Very recently, Malekzadeh and Monajjemzadeh [23] computed the nonlinear response of functionally graded plates under moving load using Newmark time integration to study the time-dependent response of plates and the influence of material gradation index, the velocity of moving load and slenderness ratio. Bellifa et al. [24] developed a new first-order shear deformation theory to analyze the bending and dynamic behavior of functionally graded plates based on the neutral surface position concept, but neglecting the effect of stretching-bending couplings. The theory developed by Bellifa et al. [24] was proved to be accurate and at the same time, simpler. Wang et al. [25] used an analytical approach to predict the thermoelastic response of functionally graded plates under transient thermal shock. The governing equations were derived using Lord and Shuman theory (L-S theory), and the material properties were considered to be varying according to a power law in the lengthwise direction.

In addition to studies mentioned above on thermomechanical analyses of FGM plates under different types of loading conditions, many researchers have also investigated the influence of piezoelectric effects on the overall response of the plates and shells, owing to their usefulness in governing and controlling the behavior of structures in real time. One of the very first studies of this sort was conducted by Tzou and Gadre [26] on a multilayered thin shell for distributed vibration control. Later, the response of a laminated composite plate, attached with a layer of piezoelectric polyvinylidene fluoride, was investigated by Jonnalgadda et al. [27] using first-order shear deformation theory. The plate was subjected to electro-thermo-mechanical loading and was analyzed for different length-to-depth and slenderness ratios. Wu et al. [28] presented a higher order theory to investigate the electromechanical response of graded piezoelectric shell structures. Numerous other attempts [29-35] have also been made by other researchers on developing the methods/techniques for determining the responses and vibration characteristics of composites bonded with piezoelectric actuators and sensors.

However, analysis of FGM plates bonded with piezoelectric actuator layers was done by Ootao and Tanigawa [36], in one of the very initial studies of this type. A three-dimensional model was developed to predict the transient response of a simply-supported plate when subjected to time-dependent temperature distribution. Liew et al. [37] conducted a study to develop a finite element formulation based on first-order shear deformation theory (FSDT) for active control of the FGM plates under a thermal gradient. A similar study was conducted by Ng et al. [38] for thin to moderately thick shells in evaluating their frequency response characteristic. Ebrahimi and Rastagoo [39] performed a study on annular FGM plates integrated with piezoelectric layers using Kirchhoff plate theory. The nonlinear free vibration response of FGM plate sandwiched between two piezoelectric actuator layers was investigated. Kapuria et al. [40] presented bending response of a layered FGM beam along with its vibration characteristics. The geometrically nonlinear analysis of bending deflection of an FGM plate bonded with piezoelectric actuator layers based on Reddy's higher order shear deformation theory was conducted by Yang, et al. [41], under transverse mechanical load in a thermoelectric environment. Reddy and Cheng [42] gave a three-dimensional solution to study the actuation of smart FGM plates which consisted of active piezoelectric material layers bonded with them. Very lately, Zhang and Zhao [43] presented a dynamic buckling analysis of a circular FGM plate in the Hamilton system, subjected

to uniform thermal shock at the lower surface. Duc et al. [44] performed nonlinear dynamic and vibration analysis of a piezoelectric FGM layer, subjected to electro-thermo-mechanical loading, using Reddy's higher-order shear deformation theory.

Research Gap

Based on the above literature review, it is very apparent that many studies have been performed on FGMs and their behavior under thermal and/or mechanical loads. Further, the sensing and actuation resulting due to the embedded piezoelectric layers on laminated composites as well as FGMs have also been studied by many researchers. Even though the procedures and results for static deflection and vibration characteristics are available in the present literature, but there are no available studies on the transient response of piezoelectric FGM plates under electro-thermo-mechanical loading.

Chapter 3

MODELING AND MATHEMATICAL FORMULATION

In this chapter, the modeling of piezoelectric FGM plate and the mathematical formulation for the FEM model are presented. The thermal analysis for obtaining temperature variation along the thickness direction and constitutive relations for the piezoelectric material are also given, before proceeding to the FEM formulation. The solution techniques used for solving the nonlinear equations and for approximating time derivatives are shown. Finally, a stepwise procedure in the form of a flow chart is also presented to solve the nonlinear dynamic plate problem.

3.1. Modeling of Smart FGM Plate

The plate considered in the present study broadly consists of two constituents, namely an FGM layer and two piezoelectric layers bonded at the top and bottom surfaces of the FGM layer, as shown in Fig. 4. Both the piezoelectric layers are identical in all respects and are made of a single isotropic and homogenous material. The FGM layer is a combination of metal and ceramic constituents, and volume fractions of these constituents are graded continuously across the thickness.

3.1.1. Modeling of the FGM layer

As discussed earlier, there are two ways suggested in literature, in which the gradation of properties in an FGM can be done, viz. the continuous variation and the stepwise variation. In the present study, the FGM layer is modeled as a single layer of continuously varying properties across the thickness. The top surface of this layer is a full ceramic surface and as we progress towards the bottom surface the volume fraction of ceramic decreases gradually and that of metal increases to become a full metal surface at the bottom. The variation of properties of FGM is governed by a power law in terms of the volume fraction of its constituents, given as below:

$$P(z) = (P_c - P_m)V_c + P_m, \tag{1}$$

where,

$$V_c = \left(\frac{z}{h} + \frac{1}{2}\right)^n.$$

Where, $P(z)$ is the value of material property in a plane located at a distance z from the midplane, h is the thickness of the FGM layer, V_c is the volume fraction of the ceramic constituent in that plane, P_c and P_m are the values of the corresponding property of ceramic and metal, respectively. Hereafter, subscripts c and m are used to represent ceramic and metal, respectively, throughout this thesis.

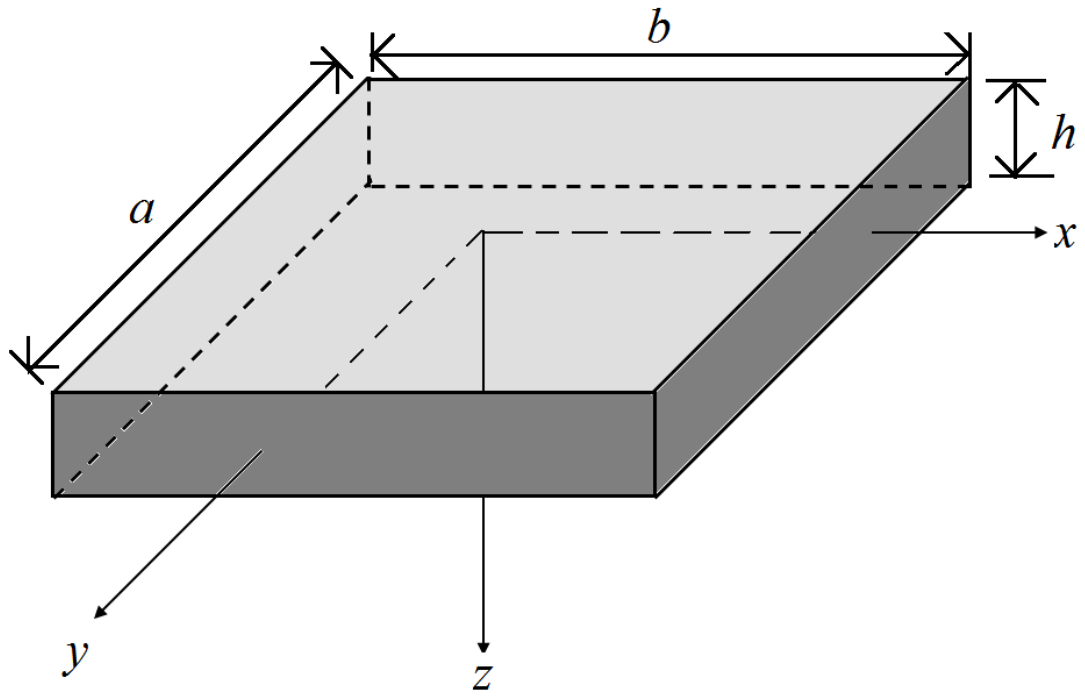

Fig. 5. The geometry of the plate showing midplane based Cartesian coordinate system.

Different values of the power law index, n are used to get different configurations of FGM layer of the plate structure. A zero value of n signifies a full ceramic composition, whereas $n = \infty$ means an entire metal composition. The variation of V_c with the non-dimensional thickness is shown in Fig. 5.

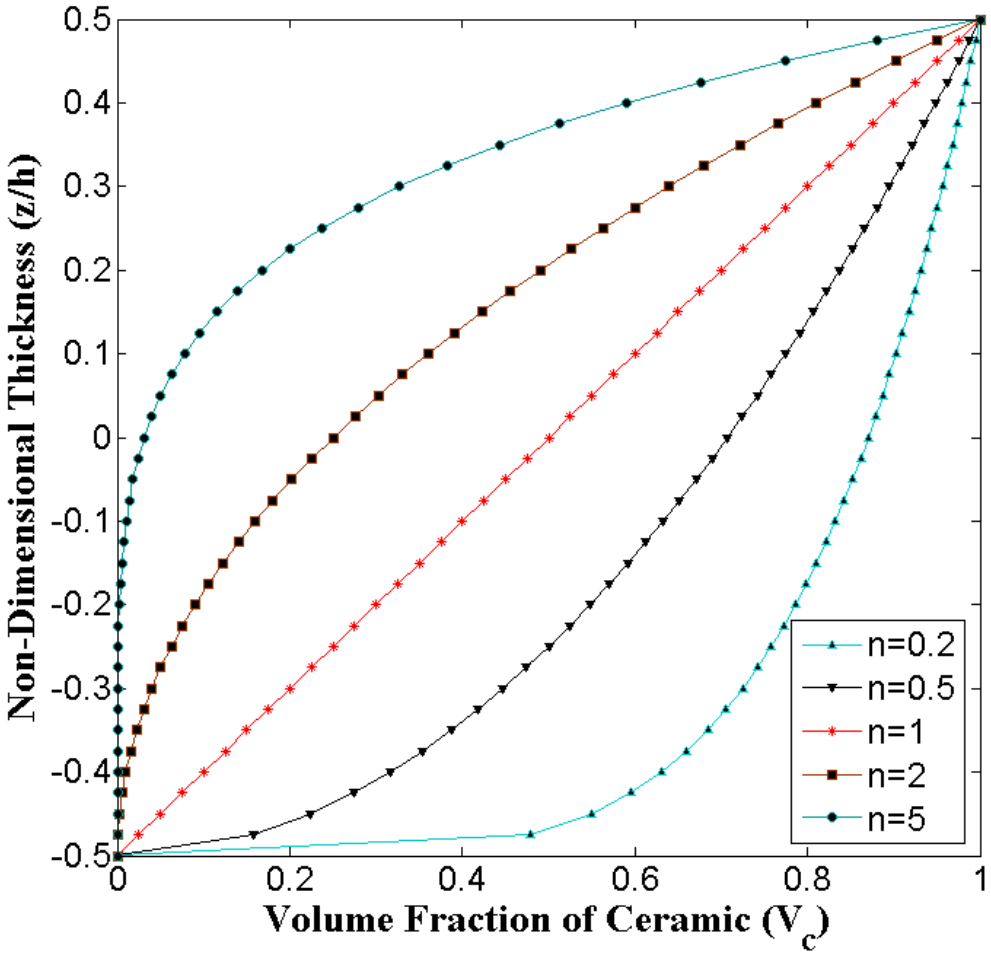

Fig. 6. Variation of ceramic volume fraction with non-dimensional thickness for different values of power law index.

3.1.2. Piezoelectric Layer

The adaptive behavior of the piezoelectric FGM plate structure is due to the piezoelectric actuator layers bonded to it. The piezoelectric materials respond to the different inputs such as mechanical loads, thermal field, electrical field, magnetic field, light source, etc.

Here, the actuator made of a one-dimensional piezoelectric material Lead Zirconate Titanate (PZT) is considered. The constitutive equations of the piezoelectric material are shown below, considering the IEEE standard notations for piezoelectricity [45].

$$D = \epsilon^T E + d_{33} T, \tag{2}$$

$$S = d_{33} E + s^E \tau \tag{3}$$

where, D is the electric displacement ($Coulomb/m^2$), ϵ^T dielectric constant or permittivity under constant stress, E is the electric field (V/m), τ is the stress (N/m^2), d_{33} is the piezoelectric constant, and the subscripts '33' means that poling of the piezoelectric material is done in the third direction (i.e., the z-axis). The piezoelectric constant has the units of m/V, or $Coulomb/Newton.S$ is the strain and s^E is the compliance for a constant electric field (inverse of Young's modulus).

3.2. Mathematical Formulation of the Problem

The piezoelectric FGM plate problem concerned in this thesis is solved for its transient response by using the finite element formulation based on Mindlin's first-order shear deformation plate theory (FSDT) and the von -Karman's geometric nonlinearity assumptions. Newton-Raphson iterative scheme is used for solving the nonlinear response of the plate, and the time-dependent response is computed by employing Newmark integration method. Before proceeding to the finite element modeling, the thermal analysis of the problem based on one-dimensional heat conduction equation is performed to compute the temperature variation across the thickness.

3.2.1. Thermal Analysis

FGM structures are engineered to withstand high-temperature gradients and thermal impacts. Usually, the ceramic side is subjected to a high temperature, and the metal side is exposed to a lower or ambient temperature. In the present study, constant temperature conditions on both the ceramic and metallic surfaces are imposed. Temperature varies along the thickness direction according to one-dimensional steady-state heat conduction equation (i.e., Fourier's law) with no variation of temperature in a plane. As per the Fourier's law, the governing equation for one dimensional heat conduction is given as:

$$\frac{d}{dz}\left[K(z)\frac{dT}{dz}\right] = 0, \tag{4}$$

subjected to,

$$T = T_c \; at \; z = \frac{h}{2}, \text{and } T = T_m \; at \; z = -\frac{h}{2}, \tag{5}$$

where, K is the thermal conductivity of the plate, which is a function of z, and T denotes the temperature.

The solution of differential Eq. (4) can be obtained using a polynomial series [46] to approximate the value of temperature on any plane located at a distance of z from the mid-plane of the plate. While taking up to seven terms in the series, it gives:

$$T(z) = T_m + \frac{\Delta T}{C}(r_1 + r_2 + r_3 + r_4 + r_5 + r_6), \tag{6}$$

where, the coefficients r_1, r_2 ... are defined as:

$$r_1 = \left(\frac{2z+h}{2h}\right); r_2 = -\frac{\Delta K}{(n+1)K_m}\left(\frac{2z+h}{2h}\right)^{n+1}; r_3 = \frac{\Delta K^2}{(2n+1)K_m^2}\left(\frac{2z+h}{2h}\right)^{2n+1};$$

$$r_4 = -\frac{\Delta K^3}{(3n+1)K_m^3}\left(\frac{2z+h}{2h}\right)^{3n+1}; r_5 = \frac{\Delta K^4}{(4n+1)K_m^4}\left(\frac{2z+h}{2h}\right)^{4n+1}; r_6 = -\frac{\Delta K^5}{(5n+1)K_m^5}\left(\frac{2z+h}{2h}\right)^{5n+1};$$

and,

$$C = 1 - \frac{\Delta K}{(n+1)K_m} + \frac{\Delta K^2}{(2n+1)K_m^2} - \frac{\Delta K^3}{(3n+1)K_m^3} + \frac{\Delta K^4}{(4n+1)K_m^4} - \frac{\Delta K^5}{(5n+1)K_m^5}\left(\frac{2z+h}{2h}\right)^{5n+1}.$$

The temperature difference between ceramic surface and metal surface is denoted as ΔT, and the difference between thermal conductivities of metal and ceramic constituents is ΔK. The temperature profile thus obtained is used in the finite element model developed in Section 3.2.6.

3.2.2. The Mindlin- Reissner Plate Theory

The Mindlin plate theory is a more generalized form of Kirchhoff's classical plate theory. Considering all the assumptions made in classical plate theory to be valid, but relaxing the normality assumption, the Mindlin plate theory takes into account the rotations of transverse normal to the midplane of the plate.

Displacement Field

Under the kinematic assumptions of the first-order shear deformation plate theory, the displacement field is expressed as [6]:

$$u(x, y, z, t) = u_0(x, y) + z\emptyset_x(x, y, t),$$

$$v(x, y, z, t) = v_0(x, y) + z\emptyset_y(x, y, t), and$$

$$w(x, y, z, t) = w_0(x, y, t), \tag{7}$$

Where, symbols u, v and w denote the displacements of a point (x, y, z), and u_0, v_0 & w_0 are the corresponding displacements of a point $(x, y, 0)$ situated on the mid-plane, along x, y and z directions, respectively; $\emptyset_x$ and $\emptyset_y$ are the angles of rotation of the transverse normal about y and x axes, respectively.

The geometrically nonlinear strains in von-Karman sense, for the above displacement field, are written as:

$$\begin{Bmatrix} \varepsilon_{xx} \\ \varepsilon_{yy} \\ \gamma_{yz} \\ \gamma_{xz} \\ \gamma_{xy} \end{Bmatrix} = \begin{Bmatrix} \varepsilon_{xx}^0 \\ \varepsilon_{yy}^0 \\ \gamma_{yz}^0 \\ \gamma_{xz}^0 \\ \gamma_{xy}^0 \end{Bmatrix} + z \begin{Bmatrix} \varepsilon_{xx}^1 \\ \varepsilon_{yy}^1 \\ 0 \\ 0 \\ \gamma_{xy}^1 \end{Bmatrix}$$

$$= \begin{Bmatrix} \dfrac{\partial u_0}{\partial x} + \dfrac{1}{2}\left(\dfrac{\partial w_0}{\partial x}\right)^2 \\ \dfrac{\partial v_0}{\partial x} + \dfrac{1}{2}\left(\dfrac{\partial w_0}{\partial y}\right)^2 \\ \dfrac{\partial w_0}{\partial y} + \emptyset_y \\ \dfrac{\partial w_0}{\partial x} + \emptyset_x \\ \dfrac{\partial u_0}{\partial y} + \dfrac{\partial v_0}{\partial x} + \dfrac{\partial w_0}{\partial x}\dfrac{\partial w_0}{\partial y} \end{Bmatrix} + z \begin{Bmatrix} \dfrac{\partial \emptyset_x}{\partial x} \\ \dfrac{\partial \emptyset_y}{\partial y} \\ 0 \\ 0 \\ \dfrac{\partial \emptyset_x}{\partial y} + \dfrac{\partial \emptyset_y}{\partial x} \end{Bmatrix}. \quad (8)$$

Weak Formulation

The principle of virtual displacement in dynamic form (Hamilton's principle) for the plate to give the governing equations of motion [47] is given as:

$$0 = \int_0^T (\delta U + \delta V - \delta K) dt, \quad (9)$$

Where, $\delta U, \delta V, \delta K$ are the virtual strain energy, virtual work done by applied force and the virtual kinetic energy, respectively and are given as:

$$\delta U^e = \int_{\Omega^e} \left\{ \int_{-\frac{h}{2}}^{\frac{h}{2}} \left[\sigma_{xx}(\delta\varepsilon_{xx}^0 + z\delta\varepsilon_{xx}^1) + \sigma_{xx}\left(\delta\varepsilon_{yy}^0 + z\delta\varepsilon_{yy}^1\right) + \sigma_{xy}\left(\delta\gamma_{xy}^0 + z\delta\gamma_{xy}^1\right) + \right.\right.$$

$$\left.\left. \sigma_{xz}\delta\gamma_{xz}^0 + \sigma_{yz}\delta\gamma_{yz}^0 \right] dz \right\} dx\, dy,$$

$$\delta V^e = -\int_{\Gamma^e}\left\{\int_{-\frac{h}{2}}^{\frac{h}{2}}[\sigma_{nn}(\delta u_{0n} + z\delta\emptyset_{\mathrm{n}}) + \sigma_{ns}(\delta u_{0s} + z\delta\emptyset_{\mathrm{s}}) + \sigma_{nz}\delta\partial w_0]\,dzds + \int_{\Omega^e}(q - kw_0)\delta w_0 dxdy\right\},$$

and,
$$\delta K = \int_{\Omega_e}\int_{-h/2}^{h/2}\rho\big[\big(\dot{u}_0 + x\dot{\phi}_x\big)\big(\delta\dot{u}_0 + x\delta\dot{\phi}_x\big) + \big(\dot{v}_0 + x\dot{\phi}_y\big)\big(\delta\dot{v}_0 + x\delta\dot{\phi}_y\big) + \dot{w}_0\delta\dot{w}_0\big]dz\,dxdy, \tag{10}$$

where, σ is used to denote the stresses, ε and γ are used for normal and shear strains respectively, and x and/or y in the subscript of a quantity denote the direction(s) of that quantity. Replacing value of energies from Eq. (10) into Eq. (9) and integrating over the thickness, we get

$$\begin{aligned}0 = \int_0^T\Bigg\{\int_{\Omega^e}\big[&N_{xx}\delta\varepsilon^0_{\mathrm{xx}} + M_{xx}\delta\varepsilon^1_{\mathrm{xx}} + N_{yy}\delta\varepsilon^0_{\mathrm{yy}} + M_{yy}\delta\varepsilon^1_{\mathrm{yy}} + N_{xy}\delta\gamma^0_{\mathrm{xy}}\\ &+ M_{xy}\delta\gamma^1_{\mathrm{xy}} + Q_x\delta\gamma^0_{\mathrm{xz}} + Q_y\delta\gamma^0_{\mathrm{yz}} + kw_0\delta w_0 - q\delta w_0\\ &- I_1\big(\dot{\emptyset}_x\delta\dot{u}_0 + \dot{\emptyset}_y\delta\dot{v}_0 + \delta\dot{\emptyset}_x\dot{u}_0 + \delta\dot{\emptyset}_y\dot{v}_0\big)\\ &- I_0(\dot{u}_0\delta\dot{u}_0 + \dot{v}_0\delta\dot{v}_0 + \dot{w}_0\delta\dot{w}_0) - I_2(\dot{\emptyset}_x\delta\dot{\emptyset}_x\\ &+ \dot{\emptyset}_y\delta\dot{\emptyset}_y)\big]dxdy\\ &- \int_{\Gamma^e}(N_{nn}\delta u_{0n} + N_{ns}\delta u_{0s} + M_{nn}\delta\emptyset_{\mathrm{n}} + M_{ns}\delta\emptyset_{\mathrm{s}}\\ &+ Q_n\delta w_0)\,ds\Bigg\}dt,\end{aligned} \tag{11}$$

where, $N$and M are used for force and moment resultants per unit area. Denoting densities of ceramic and metal constituents by $\rho_c$and ρ_m, respectively, the inertia terms I_0, I_1, I_2 can be written as:

$$\begin{Bmatrix}I_0\\I_1\\I_2\end{Bmatrix} = \int_{-h/2}^{h/2}\begin{Bmatrix}1\\z\\z^2\end{Bmatrix}[(\rho_c - \rho_m)V_c^n + \rho_m]dz. \tag{12}$$

The transverse force resultants, Q_x and Q_y are given by:

$$\begin{Bmatrix}Q_x\\Q_y\end{Bmatrix} = \int_{-\frac{h}{2}}^{\frac{h}{2}}\begin{Bmatrix}\sigma_{xz}\\\sigma_{yz}\end{Bmatrix}dz. \tag{13}$$

By solving Eq. (11), the governing equations of motion with von-Karman nonlinearity under FSDT are derived in the following form [48]:

$$\delta u_0: \quad -\left(\frac{\partial N_{xx}}{\partial x}+\frac{\partial N_{xy}}{\partial y}\right)+I_0\frac{\partial^2 u_0}{\partial t^2}+I_1\frac{\partial^2 \phi_x}{\partial t^2}=0,$$

$$\delta v_0: \quad -\left(\frac{\partial N_{xy}}{\partial x}+\frac{\partial N_{yy}}{\partial y}\right)+I_0\frac{\partial^2 v_0}{\partial t^2}+I_1\frac{\partial^2 \phi_y}{\partial t^2}=0,$$

$$\delta w_0: \quad -\left(\frac{\partial Q_x}{\partial x}+\frac{\partial Q_y}{\partial y}\right)-\mathcal{N}(u_0,v_0,w_0)-q+I_0\frac{\partial^2 w_0}{\partial t^2}=0,$$

$$\delta \phi_x: \quad -\left(\frac{\partial M_{xx}}{\partial x}+\frac{\partial M_{xy}}{\partial y}\right)+Q_x+I_2\frac{\partial^2 \phi_x}{\partial t^2}+I_1\frac{\partial^2 u_0}{\partial t^2}=0,$$

$$\delta \phi_y: \quad -\left(\frac{\partial M_{xy}}{\partial x}+\frac{\partial M_{yy}}{\partial y}\right)+Q_y+I_2\frac{\partial^2 \phi_y}{\partial t^2}+I_1\frac{\partial^2 v_0}{\partial t^2}=0, \tag{14}$$

where, $\mathcal{N}(u_0,v_0,w_0)=\frac{\partial}{\partial x}\left(N_{xx}\frac{\partial w_0}{\partial x}+N_{xy}\frac{\partial w_0}{\partial y}\right)+\frac{\partial}{\partial y}\left(N_{xy}\frac{\partial w_0}{\partial x}+N_{yy}\frac{\partial w_0}{\partial y}\right)$ and the force and moment resultants per unit area are given as:

$$\begin{Bmatrix}N_{xx}\\N_{yy}\\N_{xx}\end{Bmatrix}=\begin{bmatrix}A_{11}&A_{12}&A_{16}\\A_{12}&A_{22}&A_{26}\\A_{16}&A_{26}&A_{66}\end{bmatrix}\begin{Bmatrix}\frac{\partial u_0}{\partial x}+\frac{1}{2}\left(\frac{\partial w_0}{\partial x}\right)^2\\\frac{\partial v_0}{\partial y}+\frac{1}{2}\left(\frac{\partial w_0}{\partial y}\right)^2\\\frac{\partial u_0}{\partial y}+\frac{\partial v_0}{\partial x}+\frac{\partial w_0}{\partial x}\frac{\partial w_0}{\partial y}\end{Bmatrix}+\begin{bmatrix}B_{11}&B_{12}&B_{16}\\B_{12}&B_{22}&B_{26}\\B_{16}&B_{26}&B_{66}\end{bmatrix}\begin{Bmatrix}\frac{\partial \phi_x}{\partial x}\\\frac{\partial \phi_y}{\partial y}\\\frac{\partial \phi_x}{\partial y}+\frac{\partial \phi_y}{\partial x}\end{Bmatrix}-\begin{Bmatrix}N_{xx}^T\\N_{yy}^T\\N_{xy}^T\end{Bmatrix}-\begin{Bmatrix}N_{xx}^P\\N_{yy}^P\\N_{xy}^P\end{Bmatrix}, \tag{15}$$

$$\begin{Bmatrix} M_{xx} \\ M_{yy} \\ M_{xx} \end{Bmatrix} = \begin{bmatrix} B_{11} & B_{12} & B_{16} \\ B_{12} & B_{22} & B_{26} \\ B_{16} & B_{26} & B_{66} \end{bmatrix} \begin{Bmatrix} \dfrac{\partial u_0}{\partial x} + \dfrac{1}{2}\left(\dfrac{\partial w_0}{\partial x}\right)^2 \\ \dfrac{\partial v_0}{\partial y} + \dfrac{1}{2}\left(\dfrac{\partial w_0}{\partial y}\right)^2 \\ \dfrac{\partial u_0}{\partial y} + \dfrac{\partial v_0}{\partial x} + \dfrac{\partial w_0}{\partial x}\dfrac{\partial w_0}{\partial y} \end{Bmatrix} + \begin{bmatrix} D_{11} & D_{12} & D_{16} \\ D_{12} & D_{22} & D_{26} \\ D_{16} & D_{26} & D_{66} \end{bmatrix} \begin{Bmatrix} \dfrac{\partial \emptyset_x}{\partial x} \\ \dfrac{\partial \emptyset_y}{\partial y} \\ \dfrac{\partial \emptyset_x}{\partial y} + \dfrac{\partial \emptyset_y}{\partial x} \end{Bmatrix} - \begin{Bmatrix} M_{xx}^T \\ M_{yy}^T \\ M_{xy}^T \end{Bmatrix} - \begin{Bmatrix} M_{xx}^P \\ M_{yy}^P \\ M_{xy}^P \end{Bmatrix}, \tag{16}$$

$$\begin{Bmatrix} Q_y \\ Q_x \end{Bmatrix} = K_s \begin{bmatrix} A_{44} & A_{45} \\ A_{45} & A_{55} \end{bmatrix} \begin{Bmatrix} \dfrac{\partial w_0}{\partial y} + \emptyset_y \\ \dfrac{\partial w_0}{\partial x} + \emptyset_x \end{Bmatrix} - \begin{Bmatrix} Q_y^P \\ Q_x^P \end{Bmatrix}, \tag{17}$$

$$\begin{Bmatrix} Q_x^P \\ Q_y^P \end{Bmatrix} = \sum_{K=1}^{N} \int_{z_k}^{z_{k+1}} \begin{bmatrix} \bar{e}_{14} & \bar{e}_{24} & 0 \\ \bar{e}_{15} & \bar{e}_{25} & 0 \end{bmatrix}^{(k)} \begin{Bmatrix} \varepsilon_x \\ \varepsilon_y \\ \varepsilon_z \end{Bmatrix}^{(k)} dz, \tag{18}$$

where, $\bar{e}_{ij}$are the transformed piezoelectric coefficients, k_s is the shear correction coefficient, and matrices $[A_{ij}], [B_{ij}]$and $[D_{ij}]$, for $i,j = 1,2,6$ represent the inplane, bending-stretching coupling, and bending stiffness matrices, respectively, and $[A_{ij}]$ for $i,j = 4,5$ represents thickness-shear stiffness matrix [14]. The values of these stiffnesses are computed in terms of effective moduli of the FGM as

$$A_{ij} = \begin{cases} \displaystyle\int_{-h/2}^{h/2} \left(\left(Q_{ij}^c - Q_{ij}^m\right)\left(\frac{2z+h}{2h}\right)^n + Q_{ij}^m \right) dz, & i,j = 1,2,6 \\ \displaystyle\int_{-h/2}^{h/2} k_i k_j \left(\left(Q_{ij}^c - Q_{ij}^m\right)\left(\frac{2z+h}{2h}\right)^n + Q_{ij}^m \right) dz, & i,j = 4,5 \end{cases}$$

and, $$\left(B_{ij}, D_{ij}\right) = \int_{-h/2}^{h/2} \left\{ \left(Q_{ij}^c - Q_{ij}^m\right)\left(\frac{2z+h}{2h}\right)^n (z, z^2) + Q_{ij}^m (z, z^2) \right\} dz \tag{19}$$

The thermal and piezoelectric force and moment resultants, $N^T, M^T \; and \; N^P, M^P$ are given as

$$\{N^T\} = \sum_{k=1}^{N} \int_{z_k}^{z_{k+1}} [\bar{Q}]^{(k)} \{\overline{\alpha}\}^{(k)} \Delta T dz$$

$$\{M^T\} = \sum_{k=1}^{N} \int_{z_k}^{z_{k+1}} [\bar{Q}]^{(k)} \{\overline{\alpha}\}^{(k)} \Delta T z dz \tag{20}$$

and,

$$\{N^P\} = \sum_{k=1}^{N} \int_{z_k}^{z_{k+1}} [\bar{e}]^{(k)} \{E\}^{(k)} dz$$

$$\{M^P\} = \sum_{k=1}^{N} \int_{z_k}^{z_{k+1}} [\overline{e}]^{(k)} \{E\}^{(k)} z dz \tag{21}$$

3.2.3. Virtual Work Statement

Using Eq, (5), the virtual work statement can be written as the following five weak form

$$0 = \int_{\Omega^e} \left(\frac{\partial \delta u_0}{\partial x} N_{xx} + \frac{\partial \delta u_0}{\partial y} N_{xy} \right) dxdy - \oint_{\Gamma^e} \left(N_{xx} n_x + N_{xy} n_y \right) \delta u_0 ds,$$

$$0 = \int_{\Omega^e} \left(\frac{\partial \delta v_0}{\partial x} N_{xy} + \frac{\partial \delta v_0}{\partial y} N_{yy} \right) dxdy - \oint_{\Gamma^e} \left(N_{xy} n_x + N_{yy} n_y \right) \delta v_0 ds,$$

$$0 = \int_{\Omega^e} \left[\frac{\partial \delta w_0}{\partial x} Q_x + \frac{\partial \delta w_0}{\partial y} Q_y + \frac{\partial \delta w_0}{\partial x} \left(N_{xx} \frac{\partial w_0}{\partial x} + N_{xy} \frac{\partial w_0}{\partial y} \right) + \frac{\partial \delta w_0}{\partial y} \left(N_{xy} \frac{\partial w_0}{\partial x} + N_{yy} \frac{\partial w_0}{\partial y} \right) - \delta w_0 q + k w_0 \delta w_0 \right] dxdy - \oint_{\Gamma^e} \left[\left(Q_x + N_{xx} \frac{\partial w_0}{\partial x} + N_{xy} \frac{\partial w_0}{\partial y} \right) n_x + \left(Q_y + N_{xy} \frac{\partial w_0}{\partial x} + N_{yy} \frac{\partial w_0}{\partial y} \right) n_y \right] \delta w_0 ds,$$

$$0 = \int_{\Omega^e} \left(\frac{\partial \delta \emptyset_x}{\partial x} M_{xx} + \frac{\partial \delta \emptyset_x}{\partial y} M_{xy} + \delta \emptyset_x Q_x \right) dxdy - \oint_{\Gamma^e} \left(M_{xx} n_x + M_{xy} n_y \right) \delta \emptyset_x ds$$

$$0 = \int_{\Omega^e} \left(\frac{\partial \delta \emptyset_y}{\partial x} M_{xy} + \frac{\partial \delta \emptyset_y}{\partial y} M_{yy} + \delta \emptyset_y Q_y \right) dxdy - \oint_{\Gamma^e} \left(M_{xy} n_y + M_{yy} n_y \right) \delta \emptyset_y ds. \quad (22)$$

The secondary variables of the formulation are identified as,

$$\widehat{N}_n \equiv N_{xx} n_x + N_{xy} n_y, \ \widehat{N}_s \equiv N_{xy} n_x + N_{yy} n_y$$

$$\widehat{M}_n \equiv M_{xx} n_x + M_{xy} n_y, \ \widehat{M}_s \equiv M_{xy} n_x + M_{yy} n_y$$

and, $$\widehat{Q}_n \equiv \left(Q_x + N_{xx} \frac{\partial w_0}{\partial x} + N_{xy} \frac{\partial w_0}{\partial y} \right) n_x + \left(Q_y + N_{xy} \frac{\partial w_0}{\partial x} + N_{yy} \frac{\partial w_0}{\partial y} \right) n_y. \quad (23)$$

3.2.4. Finite Element Model

The virtual work statements in Eq. (22) contains 1st order derivatives of the dependent variables. Therefore, they can be approximated by using Lagrange interpolation functions.

$$u_0(x,y) = \sum_{j=1}^{m} u_j \psi_j^{(1)}(x,y), \quad v_0(x,y) = \sum_{j=1}^{m} v_j \psi_j^{(1)}(x,y),$$

$$w_0(x,y) = \sum_{j=1}^{n} w_j \psi_j^{(2)}(x,y) \quad (24)$$

$$\phi_x(x,y) = \sum_{j=1}^{p} S_j^{(1)} \psi_j^{(3)}(x,y), \quad \phi_y(x,y) = \sum_{j=1}^{p} S_j^{(2)} \psi_j^{(3)}(x,y) \quad (25)$$

Where $\psi_j^{(\alpha)}$ is Lagrange interpolation function.

Substituting Eqs. (24-25) into Eq. (22), we get a finite element model:

$$\begin{bmatrix} [K^{11}] & [K^{12}] & [K^{13}] & [K^{14}] & [K^{15}] \\ [K^{21}] & [K^{22}] & [K^{23}] & [K^{24}] & [K^{25}] \\ [K^{31}] & [K^{32}] & [K^{33}] & [K^{34}] & [K^{35}] \\ [K^{41}] & [K^{42}] & [K^{43}] & [K^{44}] & [K^{45}] \\ [K^{51}] & [K^{52}] & [K^{53}] & [K^{54}] & [K^{55}] \end{bmatrix} \begin{Bmatrix} \{u^e\} \\ \{v^e\} \\ \{w^e\} \\ \{S^1\} \\ \{S^2\} \end{Bmatrix} = \begin{Bmatrix} \{F^1\} \\ \{F^2\} \\ \{F^3\} \\ \{F^4\} \\ \{F^5\} \end{Bmatrix} + \begin{Bmatrix} \{F^{1T}\} \\ \{F^{2T}\} \\ \{F^{3T}\} \\ \{F^{4T}\} \\ \{F^{5T}\} \end{Bmatrix} + \begin{Bmatrix} \{F^{1P}\} \\ \{F^{2P}\} \\ \{F^{3P}\} \\ \{F^{4P}\} \\ \{F^{5P}\} \end{Bmatrix}$$

$$[K^e]\{\Delta^e\} = \{F^e\}, \tag{26}$$

where the coefficients of sub-matrices $[K^{\alpha\beta}]$ and vectors $\{F^{\alpha}\}$ and $\{F^{\alpha T}\}$ are given as

$$K_{ij}^{11} = \int_{\Omega^e} \left[A_{11} \frac{\partial \psi_i}{\partial x} \frac{\partial \psi_j}{\partial x} + A_{66} \frac{\partial \psi_i}{\partial y} \frac{\partial \psi_j}{\partial y} + A_{16} \left(\frac{\partial \psi_i}{\partial x} \frac{\partial \psi_j}{\partial y} + \frac{\partial \psi_i}{\partial y} \frac{\partial \psi_j}{\partial x} \right) \right] dxdy,$$

$$K_{ij}^{12} = \int_{\Omega^e} \left[A_{12} \frac{\partial \psi_i}{\partial x} \frac{\partial \psi_j}{\partial y} + A_{66} \frac{\partial \psi_i}{\partial y} \frac{\partial \psi_j}{\partial x} + A_{26} \frac{\partial \psi_i}{\partial y} \frac{\partial \psi_j}{\partial y} + A_{16} \frac{\partial \psi_i}{\partial x} \frac{\partial \psi_j}{\partial x} \right] dxdy = K_{ji}^{21},$$

$$\begin{aligned} K_{ij}^{13} = \frac{1}{2} \int_{\Omega^e} \Bigg\{ & \frac{\partial \psi_i}{\partial x} \left[A_{11} \frac{\partial w_0}{\partial x} \frac{\partial \psi_j}{\partial x} + A_{12} \frac{\partial w_0}{\partial y} \frac{\partial \psi_j}{\partial y} + A_{16} \left(\frac{\partial w_0}{\partial x} \frac{\partial \psi_j}{\partial y} + \frac{\partial w_0}{\partial y} \frac{\partial \psi_j}{\partial x} \right) \right] \\ & + \frac{\partial \psi_i}{\partial y} \Bigg[A_{16} \frac{\partial w_0}{\partial x} \frac{\partial \psi_j}{\partial x} + A_{26} \frac{\partial w_0}{\partial y} \frac{\partial \psi_j}{\partial y} \\ & + A_{66} \left(\frac{\partial w_0}{\partial x} \frac{\partial \psi_j}{\partial y} + \frac{\partial w_0}{\partial y} \frac{\partial \psi_j}{\partial x} \right) \Bigg] \Bigg\} dxdy, \end{aligned}$$

$$K_{ij}^{14} = \int_{\Omega^e} \left[\frac{\partial \psi_i}{\partial x} \left(B_{11} \frac{\partial \psi_j}{\partial x} + B_{16} \frac{\partial \psi_j}{\partial y} \right) + \frac{\partial \psi_i}{\partial y} \left(B_{16} \frac{\partial \psi_j}{\partial x} + B_{66} \frac{\partial \psi_j}{\partial y} \right) \right] dxdy = K_{ji}^{41},$$

$$K_{ij}^{15} = \int_{\Omega^e} \left[\frac{\partial \psi_i}{\partial x} \left(B_{16} \frac{\partial \psi_j}{\partial x} + B_{12} \frac{\partial \psi_j}{\partial y} \right) + \frac{\partial \psi_i}{\partial y} \left(B_{66} \frac{\partial \psi_j}{\partial x} + B_{26} \frac{\partial \psi_j}{\partial y} \right) \right] dxdy = K_{ji}^{51},$$

$$K_{ij}^{22} = \int_{\Omega^e} \left[A_{22} \frac{\partial \psi_i}{\partial y} \frac{\partial \psi_j}{\partial y} + A_{66} \frac{\partial \psi_i}{\partial x} \frac{\partial \psi_j}{\partial x} + A_{26} \left(\frac{\partial \psi_i}{\partial x} \frac{\partial \psi_j}{\partial y} + \frac{\partial \psi_i}{\partial y} \frac{\partial \psi_j}{\partial x} \right) \right] dxdy,$$

$$K_{ij}^{23} = \frac{1}{2}\int_{\Omega^e}\left\{\frac{\partial\psi_i}{\partial y}\left[A_{12}\frac{\partial w_0}{\partial x}\frac{\partial\psi_j}{\partial x} + A_{22}\frac{\partial w_0}{\partial y}\frac{\partial\psi_j}{\partial y} + A_{26}\left(\frac{\partial w_0}{\partial x}\frac{\partial\psi_j}{\partial y} + \frac{\partial w_0}{\partial y}\frac{\partial\psi_j}{\partial x}\right)\right]\right.$$
$$+ \frac{\partial\psi_i}{\partial x}\left[A_{16}\frac{\partial w_0}{\partial x}\frac{\partial\psi_j}{\partial x} + A_{26}\frac{\partial w_0}{\partial y}\frac{\partial\psi_j}{\partial y}\right.$$
$$\left.\left. + A_{66}\left(\frac{\partial w_0}{\partial x}\frac{\partial\psi_j}{\partial y} + \frac{\partial w_0}{\partial y}\frac{\partial\psi_j}{\partial x}\right)\right]\right\} dxdy,$$

$$K_{ij}^{24} = \int_{\Omega^e}\left[\frac{\partial\psi_i}{\partial y}\left(B_{12}\frac{\partial\psi_j}{\partial x} + B_{26}\frac{\partial\psi_j}{\partial y}\right) + \frac{\partial\psi_i}{\partial x}\left(B_{16}\frac{\partial\psi_j}{\partial x} + B_{66}\frac{\partial\psi_j}{\partial y}\right)\right] dxdy = K_{ji}^{42},$$

$$K_{ij}^{25} = \int_{\Omega^e}\left[\frac{\partial\psi_i}{\partial y}\left(B_{26}\frac{\partial\psi_j}{\partial x} + B_{22}\frac{\partial\psi_j}{\partial y}\right) + \frac{\partial\psi_i}{\partial x}\left(B_{66}\frac{\partial\psi_j}{\partial x} + B_{26}\frac{\partial\psi_j}{\partial y}\right)\right] dxdy = K_{ji}^{52},$$

$$K_{ij}^{31} = \int_{\Omega^e}\left\{\frac{\partial\psi_j}{\partial x}\left[A_{11}\frac{\partial w_0}{\partial x}\frac{\partial\psi_i}{\partial x} + A_{12}\frac{\partial w_0}{\partial y}\frac{\partial\psi_i}{\partial y} + A_{16}\left(\frac{\partial w_0}{\partial x}\frac{\partial\psi_i}{\partial y} + \frac{\partial w_0}{\partial y}\frac{\partial\psi_i}{\partial x}\right)\right]\right.$$
$$+ \frac{\partial\psi_j}{\partial y}\left[A_{16}\frac{\partial w_0}{\partial x}\frac{\partial\psi_i}{\partial x} + A_{26}\frac{\partial w_0}{\partial y}\frac{\partial\psi_i}{\partial y}\right.$$
$$\left.\left. + A_{66}\left(\frac{\partial w_0}{\partial x}\frac{\partial\psi_i}{\partial y} + \frac{\partial w_0}{\partial y}\frac{\partial\psi_i}{\partial x}\right)\right]\right\} dxdy,$$

$$K_{ij}^{32} = \int_{\Omega^e}\left\{\frac{\partial\psi_i}{\partial y}\left[A_{12}\frac{\partial w_0}{\partial x}\frac{\partial\psi_i}{\partial x} + A_{22}\frac{\partial w_0}{\partial y}\frac{\partial\psi_i}{\partial y} + A_{26}\left(\frac{\partial w_0}{\partial x}\frac{\partial\psi_i}{\partial y} + \frac{\partial w_0}{\partial y}\frac{\partial\psi_i}{\partial x}\right)\right]\right.$$
$$+ \frac{\partial\psi_j}{\partial x}\left[A_{16}\frac{\partial w_0}{\partial x}\frac{\partial\psi_i}{\partial x} + A_{26}\frac{\partial w_0}{\partial y}\frac{\partial\psi_i}{\partial y}\right.$$
$$\left.\left. + A_{66}\left(\frac{\partial w_0}{\partial x}\frac{\partial\psi_i}{\partial y} + \frac{\partial w_0}{\partial y}\frac{\partial\psi_i}{\partial x}\right)\right]\right\} dxdy,$$

$$K_{ij}^{33} = K_s \int_{\Omega^e} \left[\frac{\partial \psi_i}{\partial x} \left(A_{55} \frac{\partial \psi_j}{\partial x} + A_{45} \frac{\partial \psi_j}{\partial y} \right) + \frac{\partial \psi_i}{\partial y} \left(A_{45} \frac{\partial \psi_j}{\partial x} + A_{44} \frac{\partial \psi_j}{\partial y} \right) \right] dxdy$$
$$+ \frac{1}{2} \int_{\Omega^e} \left\{ \left[A_{11} \left(\frac{\partial w_0}{\partial x} \right)^2 + A_{12} \left(\frac{\partial w_0}{\partial y} \right)^2 + 2A_{16} \frac{\partial w_0}{\partial x} \frac{\partial w_0}{\partial y} \right] \frac{\partial \psi_i}{\partial x} \frac{\partial \psi_j}{\partial x} \right.$$
$$+ \left[A_{16} \left(\frac{\partial w_0}{\partial x} \right)^2 + A_{26} \left(\frac{\partial w_0}{\partial y} \right)^2 + 2A_{66} \frac{\partial w_0}{\partial x} \frac{\partial w_0}{\partial y} \right] \left(\frac{\partial \psi_i}{\partial x} \frac{\partial \psi_j}{\partial y} \right.$$
$$\left. + \frac{\partial \psi_j}{\partial x} \frac{\partial \psi_i}{\partial y} \right)$$
$$\left. + \left[A_{12} \left(\frac{\partial w_0}{\partial x} \right)^2 + A_{22} \left(\frac{\partial w_0}{\partial y} \right)^2 + 2A_{26} \frac{\partial w_0}{\partial x} \frac{\partial w_0}{\partial y} \right] \frac{\partial \psi_i}{\partial y} \frac{\partial \psi_J}{\partial y} \right\} dxdy,$$

$$K_{ij}^{34} = K_s \int_{\Omega^e} \left(A_{55} \frac{\partial \psi_i}{\partial x} \psi_j + A_{45} \frac{\partial \psi_i}{\partial y} \psi_i \right) dxdy$$
$$+ \int_{\Omega^e} \left\{ \frac{\partial \psi_i}{\partial x} \left[\frac{\partial w_0}{\partial x} \left(B_{11} \frac{\partial \psi_j}{\partial x} + B_{16} \frac{\partial \psi_j}{\partial y} \right) + \frac{\partial w_0}{\partial y} \left(B_{16} \frac{\partial \psi_j}{\partial x} + B_{66} \frac{\partial \psi_j}{\partial y} \right) \right] \right.$$
$$+ \frac{\partial \psi_i}{\partial y} \left[\frac{\partial w_0}{\partial y} \left(B_{12} \frac{\partial \psi_i}{\partial x} + B_{26} \frac{\partial \psi_j}{\partial y} \right) \right.$$
$$\left. \left. + \frac{\partial w_0}{\partial x} \left(B_{16} \frac{\partial \psi_j}{\partial x} + B_{66} \frac{\partial \psi_j}{\partial y} \right) \right] \right\} dxdy,$$

$$K_{ij}^{35} = K_s \int_{\Omega^e} \left(A_{45} \frac{\partial \psi_i}{\partial x} \psi_j + A_{44} \frac{\partial \psi_i}{\partial y} \psi_j \right) dxdy$$
$$+ \int_{\Omega^e} \left\{ \frac{\partial \psi_i}{\partial x} \left[\frac{\partial w_0}{\partial x} \left(B_{12} \frac{\partial \psi_j}{\partial y} + B_{16} \frac{\partial \psi_j}{\partial x} \right) + \frac{\partial w_0}{\partial y} \left(B_{26} \frac{\partial \psi_j}{\partial y} + B_{66} \frac{\partial \psi_j}{\partial x} \right) \right] \right.$$
$$+ \frac{\partial \psi_i}{\partial y} \left[\frac{\partial w_0}{\partial y} \left(B_{22} \frac{\partial \psi_i}{\partial y} + B_{26} \frac{\partial \psi_i}{\partial x} \right) \right.$$
$$\left. \left. + \frac{\partial w_0}{\partial x} \left(B_{26} \frac{\partial \psi_j}{\partial y} + B_{66} \frac{\partial \psi_j}{\partial x} \right) \right] \right\} dxdy,$$

$$K_{ij}^{43} = K_s \int_{\Omega^e} \left(A_{55} \frac{\partial \psi_j}{\partial x} \psi_i + A_{45} \frac{\partial \psi_j}{\partial y} \psi_i \right) dxdy$$
$$+ \frac{1}{2} \int_{\Omega^e} \left\{ \frac{\partial \psi_j}{\partial x} \left[\frac{\partial w_0}{\partial x} \left(B_{11} \frac{\partial \psi_i}{\partial x} + B_{16} \frac{\partial \psi_i}{\partial y} \right) \frac{\partial w_0}{\partial y} \left(B_{16} \frac{\partial \psi_i}{\partial x} + B_{66} \frac{\partial \psi_i}{\partial y} \right) \right] \right.$$
$$+ \frac{\partial \psi_j}{\partial y} \left[\frac{\partial w_0}{\partial y} \left(B_{12} \frac{\partial \psi_i}{\partial x} + B_{26} \frac{\partial \psi_i}{\partial y} \right) \right.$$
$$\left. \left. + \frac{\partial w_0}{\partial x} \left(B_{16} \frac{\partial \psi_i}{\partial x} + B_{66} \frac{\partial \psi_i}{\partial y} \right) \right] \right\} dxdy,$$

$$K_{ij}^{44} = \int_{\Omega^e} \left(D_{11} \frac{\partial \psi_i^{(3)}}{\partial x} \frac{\partial \psi_j^{(3)}}{\partial x} + D_{66} \frac{\partial \psi_i^{(3)}}{\partial y} \frac{\partial \psi_j^{(3)}}{\partial y} + K_s A_{55} \psi_i^{(3)} \psi_j^{(3)} \right) dxdy,$$

$$K_{ij}^{45} = \int_{\Omega^e} \left[\frac{\partial \psi_i}{\partial x} \left(D_{16} \frac{\partial \psi_j}{\partial x} + D_{12} \frac{\partial \psi_j}{\partial y} \right) + \frac{\partial \psi_i}{\partial y} \left(D_{66} \frac{\partial \psi_j}{\partial x} + D_{26} \frac{\partial \psi_j}{\partial y} \right) \right.$$
$$\left. + K_S A_{45} \psi_i \psi_j \right] dxdy = K_{ji}^{54},$$

$$K_{ij}^{53} = K_s \int_{\Omega^e} \left(A_{45} \frac{\partial \psi_j}{\partial x} \psi_i + A_{44} \frac{\partial \psi_j}{\partial y} \psi_i \right) dxdy$$
$$+ \frac{1}{2} \int_{\Omega^e} \left\{ \frac{\partial \psi_j}{\partial x} \left[\frac{\partial w_0}{\partial x} \left(B_{12} \frac{\partial \psi_i}{\partial y} + B_{16} \frac{\partial \psi_i}{\partial x} \right) \right.$$
$$\left. + \frac{\partial w_0}{\partial y} \left(B_{26} \frac{\partial \psi_i}{\partial y} + B_{66} \frac{\partial \psi_i}{\partial x} \right) \right]$$
$$\left. + \frac{\partial \psi_j}{\partial y} \left[\frac{\partial w_0}{\partial y} \left(B_{22} \frac{\partial \psi_i}{\partial y} + B_{26} \frac{\partial \psi_i}{\partial x} \right) + \frac{\partial w_0}{\partial x} \left(B_{26} \frac{\partial \psi_i}{\partial y} + B_{66} \frac{\partial \psi_i}{\partial x} \right) \right] \right\},$$

$$K_{ij}^{55} = \int_{\Omega^e} \left[\frac{\partial \psi_i}{\partial x} \left(D_{66} \frac{\partial \psi_j}{\partial x} + D_{26} \frac{\partial \psi_j}{\partial y} \right) + \frac{\partial \psi_j}{\partial y} \left(D_{26} \frac{\partial \psi_i}{\partial x} + D_{22} \frac{\partial \psi_i}{\partial y} \right) \right.$$
$$\left. + K_s A_{44} \psi_i \psi_j \right] dxdy,$$

and,

$$F_i^1 = \oint_{\Gamma^e}\left(N_n\psi_i^{(1)}\right)ds, \qquad F_i^2 = \oint_{\Gamma^e}\left(N_s\psi_i^{(1)}\right)ds,$$

$$F_i^3 = \int_{\Omega^e}\left(q\psi_i^{(2)}\right)dxdy + \oint_{\Gamma^e}\left(V_n\psi_i^{(2)}\right)ds,$$

$$F_i^4 = \oint_{\Gamma^e}\left(M_n\psi_i^{(3)}\right)ds, \qquad F_i^5 = \oint_{\Gamma^e}\left(M_s\psi_i^{(3)}\right)ds,$$

$$F_i^{1T} = \int_{\Omega_e}\left(N_{xx}^T\frac{\partial\psi_i^{(1)}}{\partial x} + N_{xy}^T\frac{\partial\psi_i^{(1)}}{\partial x}\right)ds,$$

$$F_i^{2T} = \int_{\Omega_e}\left(N_{yy}^T\frac{\partial\psi_i^{(1)}}{\partial y} + N_{xy}^T\frac{\partial\psi_i^{(1)}}{\partial x}\right)ds,$$

$$F_i^{3T} = \int_{\Omega^e}[\frac{\partial\psi_i^{(2)}}{\partial x}(N_{xx}^T\frac{\partial w_0}{\partial x} + N_{xy}^T\frac{\partial w_0}{\partial y}) + \frac{\partial\psi_i^{(2)}}{\partial y}(N_{xy}^T\frac{\partial w_0}{\partial x} + N_{yy}^T\frac{\partial w_0}{\partial y})]dxdy,$$

$$F_i^{4T} = \oint_{\Omega^e}\left(\frac{\partial\psi_i^{(3)}}{\partial x}M_{xx}^T\right)ds, \qquad F_i^{5T} = \oint_{\Omega^e}\left(\frac{\partial\psi_i^{(3)}}{\partial y}M_{yy}^T\right)ds,$$

$$F_i^{1P} = \int_{\Omega_e}\left(N_{xx}^P\frac{\partial\psi_i^{(1)}}{\partial x} + N_{xy}^P\frac{\partial\psi_i^{(1)}}{\partial x}\right)ds,$$

$$F_i^{2P} = \int_{\Omega_e}\left(N_{yy}^P\frac{\partial\psi_i^{(1)}}{\partial y} + N_{xy}^P\frac{\partial\psi_i^{(1)}}{\partial x}\right)ds,$$

$$F_i^{3P} = \int_{\Omega^e}[\frac{\partial\psi_i^{(2)}}{\partial x}(N_{xx}^P\frac{\partial w_0}{\partial x} + N_{xy}^P\frac{\partial w_0}{\partial y}) + \frac{\partial\psi_i^{(2)}}{\partial y}(N_{xy}^P\frac{\partial w_0}{\partial x} + N_{yy}^P\frac{\partial w_0}{\partial y})]dxdy,$$

$$F_i^{4P} = \oint_{\Omega^e} \left(\frac{\partial \psi_i^{(3)}}{\partial x} M_{xx}^P \right) ds, \qquad F_i^{5P} = \oint_{\Omega^e} \left(\frac{\partial \psi_i^{(3)}}{\partial y} M_{yy}^P \right) ds.$$

Another way of including force term associated with temperature field and piezoelectric effect, corresponding to δw_0 is by adding it into direct stiffness matrix [6]. This increases the computational efficiency because the nonlinear terms associated in w_0 associated with F^{3T} and F^{3P} require the nonlinear calculations in force vector too, but including theses terms in stiffness matrix restricts the entire nonlinear part in w_0 to stiffness matrix, thus saving the computation time.

3.3. Iterative solution techniques

3.3.1. Iterative Solution of Nonlinear Equations

The nonlinear system of algebraic equation appearing in the above finite element model is to be solved with the help of some iterative method. The basic idea involved in an iterative scheme is to reduce the nonlinear equation to a set of linear equations, and these equations are used to get an improved solution at each iteration over the previous one until some convergence criteria are satisfied. From the many iterative schemes available in the literature, the Newton-Raphson method is used in present study to get the nonlinear response of the plate structure at each load step.

Newton-Raphson Method

The most commonly used scheme in the nonlinear finite element analysis is Newton-Raphson scheme, due to the fact that it has the highest rate of convergence among all the methods available. The standard procedure for solving the nonlinear response of given plate structure is illustrated elsewhere [6, 46, 47].

The nonlinear equations have the unknown variable, i.e., displacement field at both sides of the equation, as opposed to the linear case, where the displacement can be expressed explicitly in terms of external loads and material constants [50].

$$[K]\{U\} = \{F\} \qquad (Linear\ FEA) \tag{27}$$

$$[K(U)]\{U\} = \{F(U)\} \qquad (Nonlinear\ FEA) \tag{28}$$

At any load-step, the solution by Newton-Raphson method at i^{th} iteration involves solving the equations of the following form.

$$[T^i]\{\delta U^{i+1}\} = -\{R^i\}, \tag{29}$$

where, **T** is the tangent stiffness matrix which is an indicative of stiffness of the structure in response to a small deformation in the structure. The elements of the tangent stiffness matrix are calculated as:

$$[T^i]^{\alpha\beta} = \frac{\{\delta R^i\}^{\alpha}}{\{\delta U^{i+1}\}^{\beta}} \tag{30}$$

R is the residual vector, defined as

$$R = [T]\times\{K\} - \{F\} \tag{31}$$

The change in the configuration of the system is given by

$$\delta U^{i+1} = -\frac{\{R^i\}}{[T^i]}. \tag{32}$$

The improved solution at the end of the iteration is

$$U^{i+1} = U^i + \delta U^{i+1}. \tag{33}$$

The elements of tangent stiffness matrix are given as

$$T_{ij}^{11} = K_{ij}^{11}, \quad T_{ij}^{12} = K_{ij}^{12},$$

$$T_{ij}^{13} == \frac{1}{2}\int_{\Omega^e}\left\{\frac{\partial\psi_i}{\partial x}\left[A_{11}\frac{\partial w_0}{\partial x}\frac{\partial\psi_j}{\partial x} + A_{12}\frac{\partial w_0}{\partial y}\frac{\partial\psi_j}{\partial y} + A_{16}\left(\frac{\partial w_0}{\partial x}\frac{\partial\psi_j}{\partial y} + \frac{\partial w_0}{\partial y}\frac{\partial\psi_j}{\partial x}\right)\right]\right.$$
$$+ \frac{\partial\psi_i}{\partial y}\left[A_{16}\frac{\partial w_0}{\partial x}\frac{\partial\psi_j}{\partial x} + A_{26}\frac{\partial w_0}{\partial y}\frac{\partial\psi_j}{\partial y}\right.$$
$$\left.\left. + A_{66}\left(\frac{\partial w_0}{\partial x}\frac{\partial\psi_j}{\partial y} + \frac{\partial w_0}{\partial y}\frac{\partial\psi_j}{\partial x}\right)\right]\right\}dxdy + K_{ij}^{13} = 2K_{ij}^{13},$$

$$T_{ij}^{14} = K_{ij}^{14}, \quad T_{ij}^{15} = K_{ij}^{15}, \quad T_{ij}^{21} = K_{ij}^{21}, \quad T_{ij}^{22} = K_{ij}^{22},$$

$$T_{ij}^{23} = \frac{1}{2}\int_{\Omega^e}\left\{\frac{\partial\psi_i}{\partial y}\left[A_{12}\frac{\partial w_0}{\partial x}\frac{\partial\psi_j}{\partial x} + A_{22}\frac{\partial w_0}{\partial y}\frac{\partial\psi_j}{\partial y} + A_{26}\left(\frac{\partial w_0}{\partial x}\frac{\partial\psi_j}{\partial y} + \frac{\partial w_0}{\partial y}\frac{\partial\psi_j}{\partial x}\right)\right]\right.$$
$$+ \frac{\partial\psi_i}{\partial x}\left[A_{16}\frac{\partial w_0}{\partial x}\frac{\partial\psi_j}{\partial x} + A_{26}\frac{\partial w_0}{\partial y}\frac{\partial\psi_j}{\partial y}\right.$$
$$\left.\left. + A_{66}\left(\frac{\partial w_0}{\partial x}\frac{\partial\psi_j}{\partial y} + \frac{\partial w_0}{\partial y}\frac{\partial\psi_j}{\partial x}\right)\right]\right\}dxdy + K_{ij}^{23} = 2K_{ij}^{23},$$

$$T_{ij}^{24} = K_{ij}^{24}, \quad T_{ij}^{25} = K_{ij}^{25}, \quad T_{ij}^{31} = K_{ij}^{31}, \quad T_{ij}^{32} = K_{ij}^{32},$$

$$T_{ij}^{33} = \int_{\Omega^e}\left\{\frac{\partial u_0}{\partial x}\left[A_{11}\frac{\partial\psi_j}{\partial x}\frac{\partial\psi_i}{\partial x} + A_{12}\frac{\partial\psi_j}{\partial y}\frac{\partial\psi_i}{\partial y} + A_{16}\left(\frac{\partial\psi_j}{\partial x}\frac{\partial\psi_i}{\partial y} + \frac{\partial\psi_j}{\partial y}\frac{\partial\psi_i}{\partial x}\right)\right]\right.$$
$$+ \frac{\partial u_0}{\partial y}\left[A_{16}\frac{\partial\psi_j}{\partial x}\frac{\partial\psi_i}{\partial x} + A_{26}\frac{\partial\psi_j}{\partial y}\frac{\partial\psi_i}{\partial y}\right.$$
$$\left.\left. + A_{66}\left(\frac{\partial\psi_j}{\partial x}\frac{\partial\psi_i}{\partial y} + \frac{\partial\psi_j}{\partial y}\frac{\partial\psi_i}{\partial x}\right)\right]\right\}dxdy$$
$$+ \int_{\Omega^e}\left\{\frac{\partial v_0}{\partial y}\left[A_{12}\frac{\partial\psi_j}{\partial x}\frac{\partial\psi_i}{\partial x} + A_{22}\frac{\partial\psi_j}{\partial y}\frac{\partial\psi_i}{\partial y}\right.\right.$$
$$\left. + A_{26}\left(\frac{\partial\psi_j}{\partial x}\frac{\partial\psi_i}{\partial y} + \frac{\partial\psi_j}{\partial y}\frac{\partial\psi_i}{\partial x}\right)\right]$$
$$+ \frac{\partial v_O}{\partial x}\left[A_{16}\frac{\partial\psi_j}{\partial x}\frac{\partial\psi_i}{\partial x} + A_{26}\frac{\partial\psi_j}{\partial y}\frac{\partial\psi_i}{\partial y}\right.$$
$$\left.\left. + A_{66}\left(\frac{\partial\psi_j}{\partial x}\frac{\partial\psi_i}{\partial y} + \frac{\partial\psi_j}{\partial y}\frac{\partial\psi_i}{\partial x}\right)\right]\right\}dxdy$$

$$+\int_{\Omega^e}\left\{\left[A_{11}\frac{\partial w_0}{\partial x}\frac{\partial \psi_j}{\partial x}+A_{12}\frac{\partial w_0}{\partial y}\frac{\partial \psi_i}{\partial y}+A_{16}\left(\frac{\partial w_0}{\partial x}\frac{\partial \psi_i}{\partial y}+\frac{\partial w_0}{\partial y}\frac{\partial \psi_j}{\partial x}\right)\right]\frac{\partial \psi_i}{\partial x}\frac{\partial w_0}{\partial x}\right.$$
$$+\left[A_{16}\frac{\partial w_0}{\partial x}\frac{\partial \psi_j}{\partial x}+A_{26}\frac{\partial w_0}{\partial y}\frac{\partial \psi_j}{\partial y}\right.$$
$$\left.+A_{66}\left(\frac{\partial w_0}{\partial x}\frac{\partial \psi_j}{\partial y}+\frac{\partial w_0}{\partial y}\frac{\partial \psi_j}{\partial x}\right)\right]\left(\frac{\partial \psi_i}{\partial x}\frac{\partial w_0}{\partial y}+\frac{\partial w_0}{\partial x}\frac{\partial \psi_i}{\partial y}\right)$$
$$+\left[A_{12}\frac{\partial w_0}{\partial x}\frac{\partial \psi_j}{\partial x}+A_{22}\frac{\partial w_0}{\partial y}\frac{\partial \psi_j}{\partial y}\right.$$
$$\left.\left.+A_{26}\left(\frac{\partial w_0}{\partial x}\frac{\partial \psi_j}{\partial y}+\frac{\partial w_0}{\partial y}\frac{\partial \psi_j}{\partial x}\right)\right]\frac{\partial \psi_i}{\partial y}\frac{\partial w_0}{\partial y}\right\}dxdy$$

$$+\int_{\Omega^e}\left\{\frac{\partial \psi_i}{\partial x}\left[\frac{\partial \psi_{;i}}{\partial x}\left(B_{11}\frac{\partial \phi_x}{\partial x}+B_{16}\frac{\partial \phi_x}{\partial y}\right)+\frac{\partial \psi_j}{\partial y}\left(B_{16}\frac{\partial \phi_X}{\partial x}+B_{66}\frac{\partial \phi_x}{\partial y}\right)\right]\right.$$
$$+\frac{\partial \psi_i}{\partial y}\left[\frac{\partial \psi_j}{\partial y}\left(B_{12}\frac{\partial \phi_X}{\partial x}+B_{26}\frac{\partial \phi_x}{\partial y}\right)\right.$$
$$\left.\left.+\frac{\partial \psi_j}{\partial x}\left(B_{16}\frac{\partial \phi_x}{\partial x}+B_{66}\frac{\partial \phi_X}{\partial y}\right)\right]\right\}dxdy+$$

$$\int_{\Omega^e}\left\{\frac{\partial \psi_i}{\partial x}\left[\frac{\partial \psi_j}{\partial x}\left(B_{12}\frac{\partial \phi_y}{\partial y}+B_{16}\frac{\partial \phi_y}{\partial x}\right)+\frac{\partial \psi_j}{\partial y}\left(B_{26}\frac{\partial \phi_y}{\partial y}+B_{66}\frac{\partial \phi_y}{\partial x}\right)\right]\right.$$
$$+\frac{\partial \psi_i}{\partial y}\left[\frac{\partial \psi_i}{\partial y}\left(B_{22}\frac{\partial \phi_y}{\partial y}+B_{26}\frac{\partial \phi_y}{\partial x}\right)+\frac{\partial \psi_j}{\partial x}\left(B_{26}\frac{\partial \phi_y}{\partial y}+B_{66}\frac{\partial \phi_y}{\partial x}\right)\right]$$
$$-\frac{\partial \psi_i}{\partial x}\left(N_{xx}^{T}\frac{\partial \psi_j}{\partial x}+N_{xy}^{T}\frac{\partial \psi_j}{\partial y}\right)-\frac{\partial \psi_i}{\partial y}\left(N_{xy}^{T}\frac{\partial \psi_{;j}}{\partial x}+N_{yy}^{T}\frac{\partial \psi_j}{\partial y}\right)$$
$$\left.-\frac{\partial \psi_i}{\partial x}\left(N_{xx}^{P}\frac{\partial \psi_j}{\partial x}+N_{xy}^{P}\frac{\partial \psi_j}{\partial y}\right)-\frac{\partial \psi_i}{\partial y}\left(N_{xy}^{P}\frac{\partial \psi_{;j}}{\partial x}+N_{yy}^{P}\frac{\partial \psi_j}{\partial y}\right)\right\}dxdy$$
$$+K_{ij}^{33},$$

$$T_{ij}^{34}=K_{ij}^{34},\ T_{ij}^{35}=K_{ij}^{35},\ T_{ij}^{41}=K_{ij}^{41},\quad T_{ij}^{42}=K_{ij}^{42},$$

$$T_{ij}^{43}=\frac{1}{2}\int_{\Omega^e}\left\{\frac{\partial w_0}{\partial x}\left[\frac{\partial \psi_j}{\partial x}\left(B_{11}\frac{\partial \psi_i}{\partial x}+B_{16}\frac{\partial \psi_i}{\partial y}\right)+\frac{\partial \psi_j}{\partial y}\left(B_{16}\frac{\partial \psi_i}{\partial x}+B_{66}\frac{\partial \psi_i}{\partial y}\right)\right]\right.$$
$$\left.+\frac{\partial w_0}{\partial y}\left[\frac{\partial \psi_j}{\partial y}\left(B_{12}\frac{\partial \psi_i}{\partial x}+B_{26}\frac{\partial \psi_i}{\partial y}\right)+\frac{\partial \psi_j}{\partial x}\left(B_{16}\frac{\partial \psi_i}{\partial x}+B_{66}\frac{\partial \psi_i}{\partial y}\right)\right]\right\}dxdy$$
$$+K_{i;j}^{43},$$

$$T_{ij}^{44}=K_{ij}^{44},\quad T_{ij}^{45}=K_{ij}^{45},$$

$$T_{ij}^{53} == \frac{1}{2}\int_{\Omega^e}\left\{\frac{\partial w_0}{\partial x}\left[\frac{\partial \psi_j}{\partial x}\left(B_{12}\frac{\partial \psi_i}{\partial y}+B_{16}\frac{\partial \psi_i}{\partial x}\right)+\frac{\partial \psi_j}{\partial y}\left(B_{26}\frac{\partial \psi_i}{\partial y}+B_{66}\frac{\partial \psi_i}{\partial x}\right)\right]\right.$$
$$\left.+\frac{\partial w_0}{\partial y}\left[\frac{\partial \psi_j}{\partial y}\left(B_{22}\frac{\partial \psi_i}{\partial y}+B_{26}\frac{\partial \psi_i}{\partial x}\right)+\frac{\partial \psi_j}{\partial x}\left(B_{26}\frac{\partial \psi_i}{\partial y}+B_{66}\frac{\partial \psi_i}{\partial x}\right)\right]\right\}dxdy$$
$$+K_{ij}^{53},$$

$T_{ij}^{54} = K_{ij}^{54}, and \quad T_{ij}^{55} = K_{ij}^{55}.$

3.3.2. Time Approximation of the Nonlinear Response

The response of a system in practical conditions is time dependent, as most of the systems are subjected to time-varying loads in practical conditions. In the present study, the plate is subjected to an impact load along with thermal and electrical loads. This causes an abrupt change in the configuration of the system. This abrupt change is very large in magnitude, as compared to the steady state deflection of the system under the same load, and causes the plate to vibrate. Any system under forced vibration condition has two responses, namely transient response, and steady state response. The steady state response is independent of initial conditions of the system, whereas the transient response is dependent on force. The structure in consideration here is subjected to impact load, hence the transient response lasts for a very short duration and after that steady state response prevails which is independent of time.

There are several methods suggested by many researchers for the approximation of differential equations containing time derivatives. Newmark integration is used in the present work, which is an incremental method to approximate the deflection at various time steps.

Newmark-Beta Method

The Newmark-Beta scheme employed in the present work is an unconditionally stable scheme, with constant average acceleration and the parameters $\alpha = 1/2$ and $\beta = 1/4$.

The generalized governing differential equation in structural dynamics for an element e is [48]

$$[M]\{\ddot{U}^e\} + [C^e]\{U^e\} + [K^e]\{U^e\} = \{f^e\} \tag{34}$$

In the present case there is no damping, so $[C] = 0$. Eq. (34) is reduced to a set of linear algebraic equations, relating variables at time step s and $s + 1$. From here onwards, all the equations for Newmark integration are written for e^{th} element and for the sake of brevity, superscript *e* will be omitted.

The discretized equation reduces to

$$\left[\hat{K}(\{U\}_{s+1})\right]\{U\}_{S+1} = \left\{\hat{F}\right\}_{S,S+1} \tag{35}$$

$$[\hat{K}(\{U\}_{s+1})] = [K(\{U\}_{s+1})] + a_3[M]_{s+1} \tag{36}$$

$$\{\hat{F}\}_{s,s+1} = \{F\}_{s+1} + [M]_{s+1}\{A\}_s \tag{37}$$

where,

$$\{A\}_s = a_3\{U\}_s + a_4\{U\}_s + a_5\{U\}_s,$$

and constants a_1, a_2 ... are defined as

$$a_1 = \alpha \,\Delta\, t, \quad a_2 = (1-\alpha)\,\Delta\, t, \quad a_3 = \frac{1}{\beta(\Delta\, t)^2}, \quad a_4 = a_3\,\Delta\, t, \quad a_5 = \frac{1}{\gamma} - 1.$$

Acceleration and velocity for $s + 1$ are calculated as

$$\{\ddot{U}\}_{s+1} = a_3(\{U\}_{s+1} - \{U\}_s) - a_4\{\dot{U}\} - a_5\{\ddot{U}\}_s, \tag{38}$$

$$\{\dot{U}\}_{s+1} = \{U\}_s + a_2\{\ddot{U}\}_s + a_1\{\ddot{U}\}_s. \tag{39}$$

The initial acceleration is calculated with the help of initial force condition. The force being independent of time is iterated only by adding the term containing mass matrix in Eq. (37) and the first term on right side of the equation is kept constant at every time step.

3.4. Implementation of Nonlinear Dynamic Analysis Model

The dynamic analysis of a nonlinear problem becomes more complicated, due to the fact that monitoring of solution is necessary at different time step, load step and N-R iterations. Thus, the code to be developed for dynamic analysis of a nonlinear problem needs to be a three-layer computer program. The stepwise computer implementation of the FE model developed in this section to the problem in hand is shown in Fig. 7.

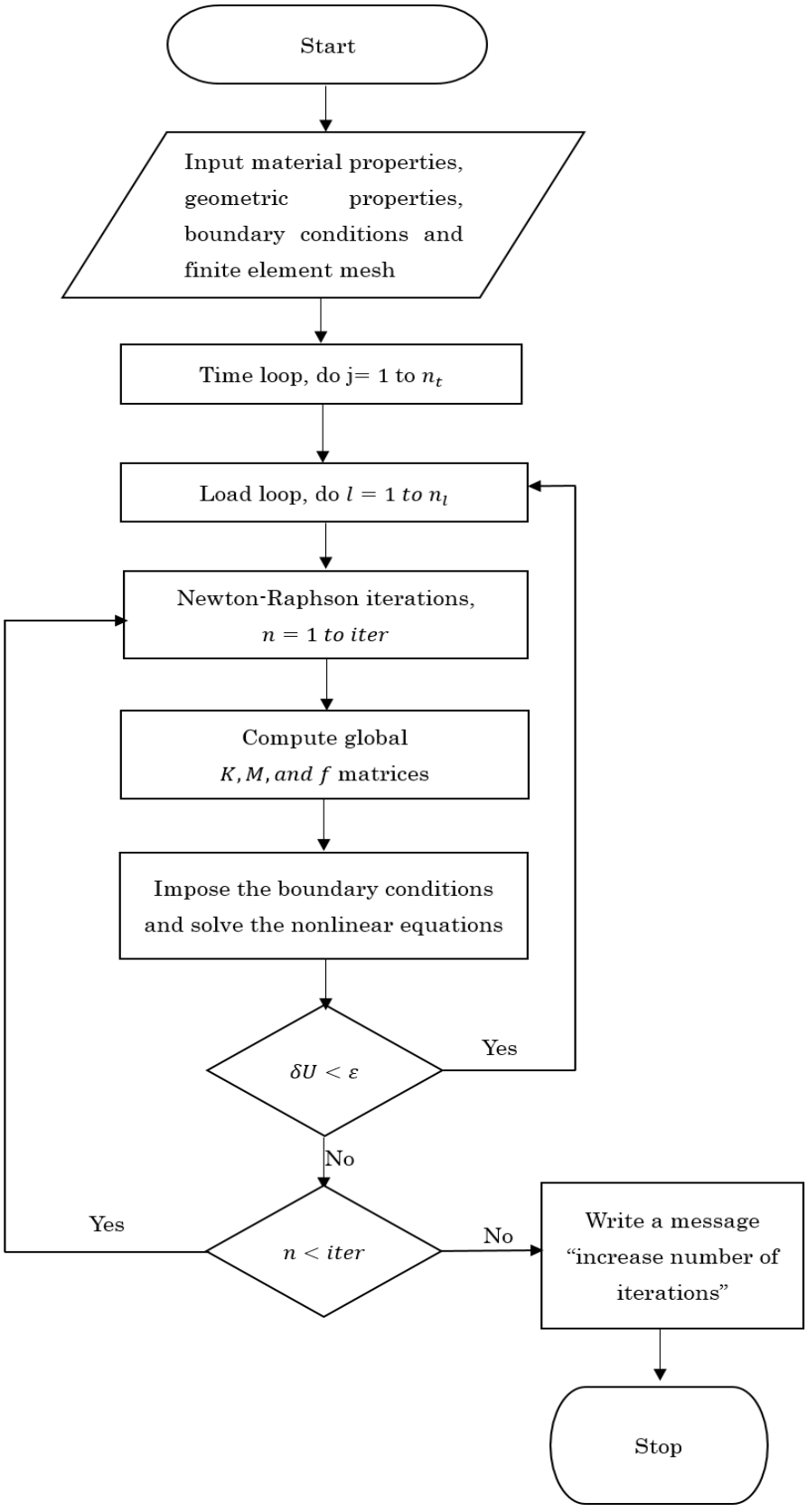

Fig. 7. Flow chart for nonlinear dynamic analysis of finite element model of the plate structure.

3.5. Boundary Conditions

In the present work, the static and dynamic responses of FGM and smart FGM rectangular plates with three different boundary conditions, as given below, are studied.

Simply-Supported Edges

$$u = 0, \quad v \neq 0, \quad w = 0, \quad \emptyset_x \neq 0, \quad \emptyset_y = 0 \quad at\ x = 0\ \&\ a;$$

$$u \neq 0, \quad v = 0, \quad w = 0, \quad \emptyset_x = 0, \quad \emptyset_y \neq 0 \quad at\ y = 0\ \&\ b.$$

Clamped Edge

$$u = 0, \quad v = 0, \quad w = 0, \quad \emptyset_x = 0, \quad \emptyset_y = 0 \quad at\ x = 0\ \&\ a;$$

$$u = 0, \quad v = 0, \quad w = 0, \quad \emptyset_x = 0, \quad \emptyset_y = 0 \quad at\ y = 0\ \&\ b.$$

Chapter 4

NUMERICAL STUDIES

In this chapter, the parametric studies are performed on the FGM and piezoelectric FGM plates, using isoparametric formulation, i.e. using the same interpolation functions for approximating both geometry of the plate and the solution. Four noded rectangular elements are used to generate the mesh, with five degrees of freedom at each node, viz. three displacements $u, v,$ and w in $x, y,$ and z directions, respectively, and two mid plane rotations ϕ_x and ϕ_y. The element considered here takes into account the shear strains as well as geometrically nonlinear strains, which requires a reduced integration to evaluate terms corresponding to these strains.

4.1. Convergence Study

The number of elements in x and y directions are fixed by conducting a convergence study for nonlinear static analysis of a simply supported square FGM plate of sides $a = b = 0.2\,m$ and subjected to a uniform impact load of $0.01\times10^6\ N/m^2$. The thickness of the plate is taken as $h = 0.01\,m$ and the value of power law index, governing the volume fractions of material constituents (aluminum-zirconia) are taken as 0.5, 1.0 and 2.0. Different uniform meshes containing different number of four-noded linear quadrilateral elements are considered for convergence study. The center deflection and load in non-dimensionalized forms used for conducting convergence study are given as:

$$Non-dimensional\ deflection = \frac{w}{h},$$

$$and\ Non-dimensional\ Load, P = \frac{qa^4}{E_m h^4}, \tag{40}$$

where, w is the center deflection of plate, h is the thickness of the plate, q is the lateral pressure applied, and E_m is the young's modulus of the metal constituent.

From the results of convergence study shown in Table 1, center deflection of FGM plate was found to be converging reasonably for a mesh of 8×8 elements. Therefore, this mesh of 8 × 8 elements is used in all the parametric studies conducted.

Table 1. Results of convergence study.

Mesh type	Non-dimensionalized center deflection		
	$n = 0.5$	$n = 1$	$n = 2$
2×2	−0.000047	−0.00052	−0.00056
4×4	−0.00058	−0.00064	−0.00070
8×8	−0.00059	−0.00066	−0.00071
10×10	−0.00059	−0.00066	−0.00071

4.2. Static Analysis

In this section, the results of static analysis of single layer FGM and piezo-bonded FGM plates under mechanical and electro-thermo-mechanical loads, respectively, are presented and discussed.

4.2.1. Static analysis of FGM Plate

The geometry and boundary conditions of the plate are shown in Fig. 8. Initially, for the validation purpose, the plate is taken as a square with sides, $a = b = 0.2\ m$ and thickness, $h = 0.01\ m$. The total load, $q = -2.2\times10^{-6}\ N/m^2$ is applied in ten steps.

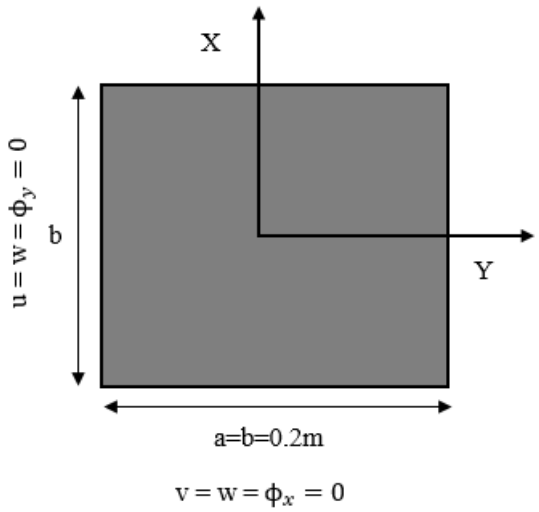

Fig. 8. Geometry and boundary conditions for the simply supported FGM plate.

The metal-ceramic combinations used for the analysis are aluminum-zirconia and aluminum-alumina, and these combinations are used throughout this thesis variably. The properties of the constituents are given in Table 2.

Table 2. Properties of FGM and Piezoelectric Constituents.

Property	Aluminum	Alumina	Zirconia	G-1195N
Young's Modulus, *E* (GPa)	70	380	151	63
Poisson's Ration	0.3	0.3	0.3	0.3
Mass Density (kg/m^3)	2707	3800	3000	7600
Thermal Conductivity (W/m-K)	204	10.4	2.09	5
Coefficient of thermal Expansion (/^{o}C)	23×10^{-6}	7.4×10^{-6}	10×10^{-6}	1.2×10^{-4}

In Fig. 9, a comparison between the results produced by the present analysis and those by Praveen and Reddy [14] is depicted. The plate is simply-supported at all the edges. It is evident from this comparison that both the results are in good agreement with each other, which verify the procedure and code used for analysis in the current work.

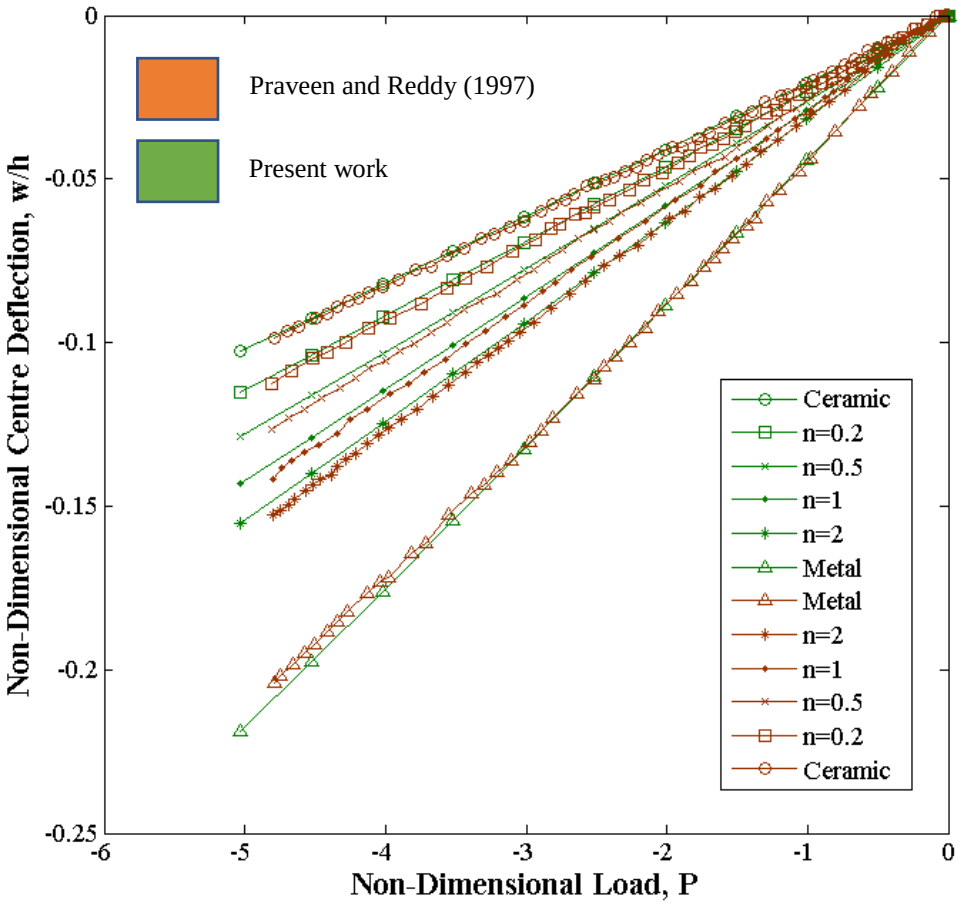

Fig. 9. Non-dimensional center deflection vs non-dimensional load for simply supported (SSSS) aluminum-zirconia FGM plate.

The variation of non-dimensional deflection with non-dimensional load for a clamped FGM plate is shown in Fig. 10 for different values of *n*. While for CSCS type boundary condition, the variation of non-dimensional center deflection with non-dimensional load is shown in Fig. 11 for different values of power law index. It can be observed from Figs. 9, 10 and 11 that there is a significant decrease in the deflection of the plate when the boundary conditions are changed from simply-supported to clamped as well as CSCS. Therefore, the manner in which a plate is mounted to the parent structure or the configuration, plays an important role in providing it structural integrity as well as deciding its response to the external loads.

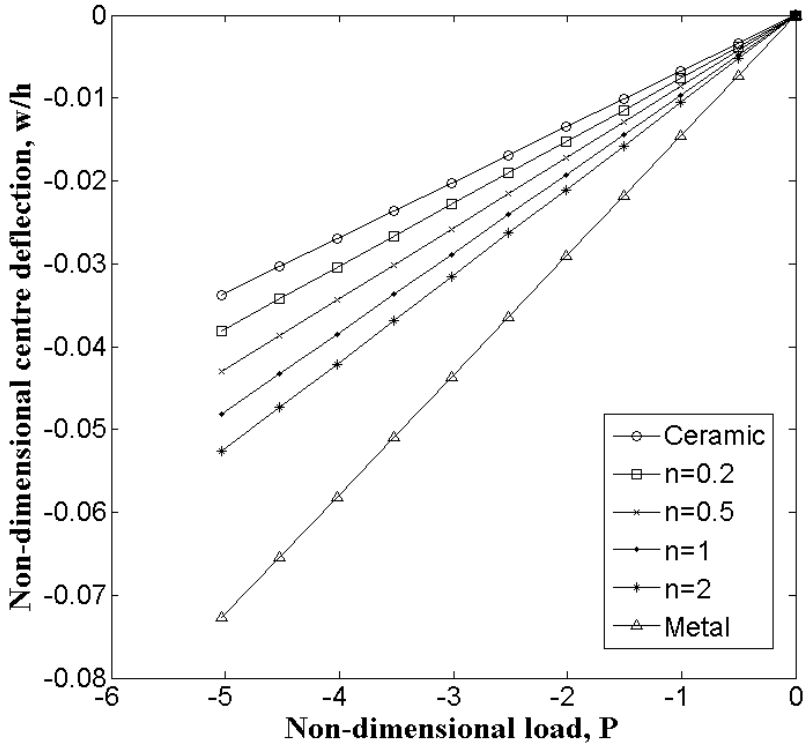

Fig. 10. Non-dimensional center deflection vs non-dimensional load for aluminum-zirconia FGM plate with all edges clamped (CCCC).

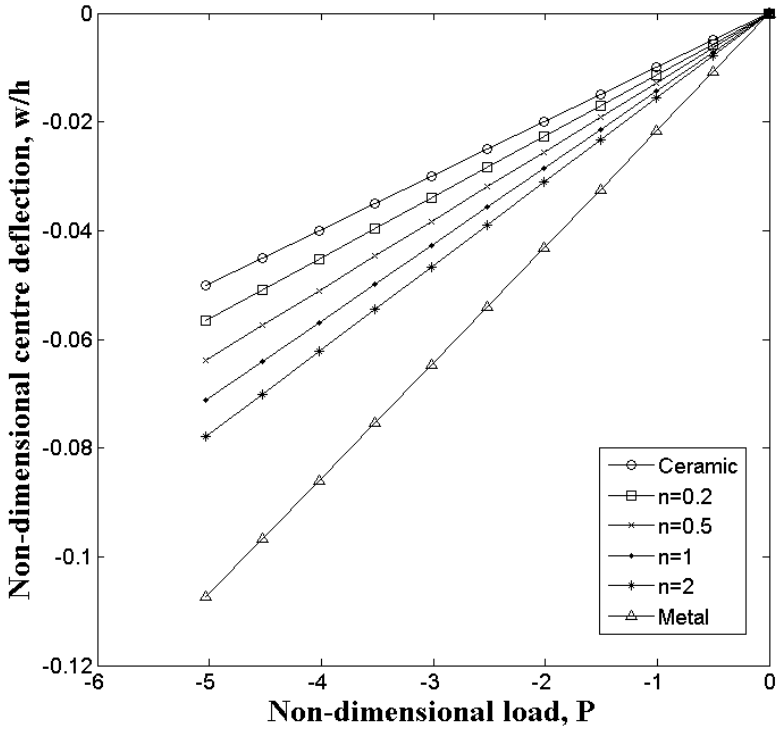

Fig. 11. Non-dimensional center deflection vs non-dimensional load for aluminum-zirconia FGM plate with boundary condition of CSCS type.

4.2.2. Smart FGM plate under electro-thermo-mechanical load

After validating the procedure for the analysis of FGM plate under static condition, the code is validated for computing the steady-state response of smart FGM plate by comparing the results with Yang et al. [41]. The plate considered has one layer of FGM (of thickness, $h = 0.01m$ $a\text{nd side} - \text{to} - \text{width ratio}, b/h = 20$) sandwiched between two layers of piezoelectric material having thickness, h_p= 0.001m. The metal-ceramic combination for FGM layer is aluminum-zirconia, and the material of piezoelectric layer is G-1195N, whose properties are given in Table 1. The temperatures specified at the top and bottom surfaces of the smart FGM plate are $300℃$ and $20℃$, respectively. The applied actuator voltage is prescribed as $-100\,V$. The plate is subjected to suddenly applied uniform lateral pressure of magnitude 11.5 MPa applied in 10 steps. The results of comparison are plotted in Fig. 12. From Fig. 12, it can be concluded that the results of present study are in agreement within reasonable limits with the results of Yang et al. [41]. Small deviations in the results can be attributed to the different theories used for applying the piezoelectric effect on the FGM plate. Yang et al. [41] used a coupled model to account for the mechanical strain effects of piezoelectric layers, whereas an uncoupled ESL model is used in the present formulation.

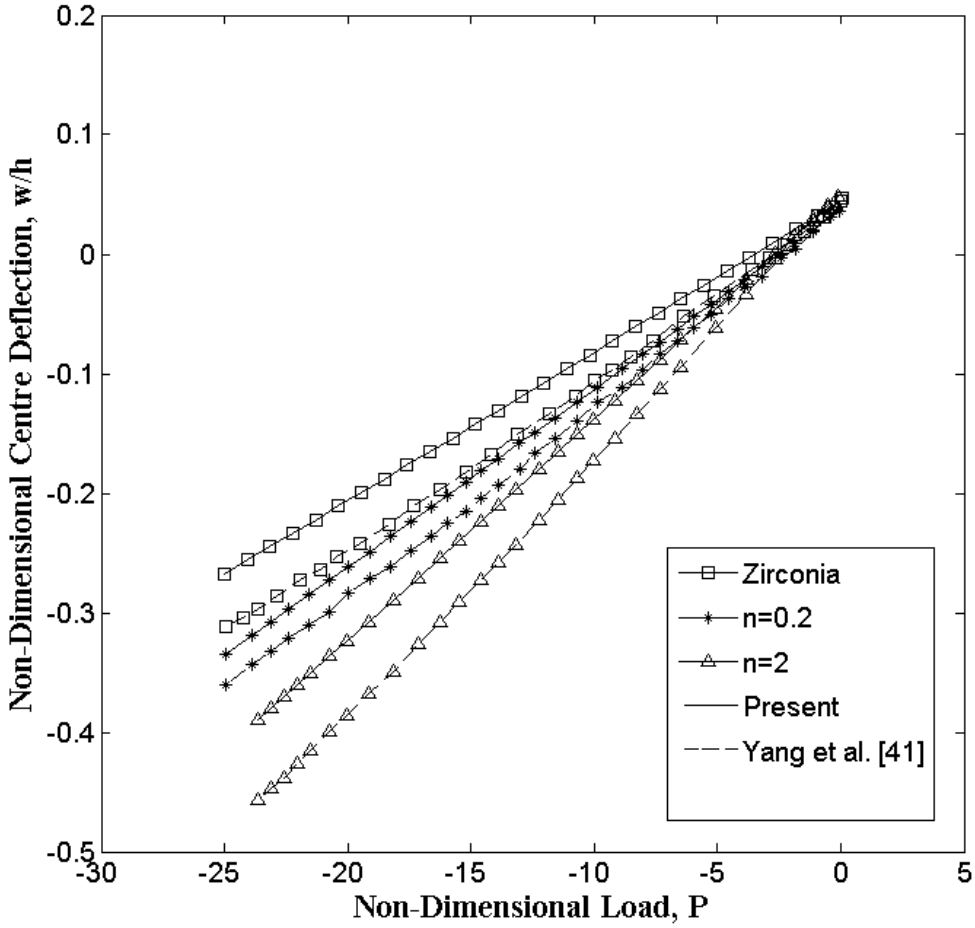

Fig. 12. Non-dimensional center deflection vs. non-dimensional load for smart FGM plate with boundary conditions of CSCS type.

4.3. Dynamic Analysis

In this section, the dynamic (i.e., transient) responses of FGM plate as well as smart FGM plate are predicted using nonlinear FEA in conjunction with unconditionally stable Newmark-Beta time integration method. Since there is no procedure available in the literature to estimate the time step for nonlinear analysis, the estimation for time step used for nonlinear transient analysis, originally derived by Leech for thin plates [51], is employed in the current study, which is given as:

$$\Delta t_1 \leq 0.25 \left(\frac{\rho h}{D}\right)^{\frac{1}{2}} (\Delta x)^2,$$

where,

$$D = [(Eh^3)/12(1-\nu^2)], \tag{41}$$

and Δx is the minimum length between two nodes.

Throughout this section, all the plots will be plotted between non-dimensionalized center node deflection and non-dimensionalized time, given as below:

$$Non-dimensionalized\ centre\ deflection, W = \frac{wE_m h}{q_0 a^2},$$

$$and\ Non-dimensionalized\ Time, t = \bar{t}\sqrt{\frac{E_m}{a^2 \rho_m}}. \qquad (42)$$

4.3.1. Transient response of FGM plate under impact load

The validity of present code developed for the transient response of aluminum-alumina FGM plate under impact load is proved by comparing the results for FGM plate presented by Praveen and Reddy [14] and those obtained in the current analysis. A simply-supported square plate of sides equal to $0.2m$ and of thickness 0.01m is analyzed for its transient response under suddenly applied uniform lateral pressure load. The uniform lateral pressure of magnitude $1\times10^{-6}\ N/m^2$ is applied over the entire surface of plate. An 8×8 uniform mesh of linear, quadrilateral elements is used for discretizing the whole domain, and a time step of $0.00001s$ is used to perform the analysis. The results of comparison for different values of material power law exponent n are plotted in Fig. 13. As noted from Fig. 13 that the results produced by both the studies are in absolute match with each other.

Effects of different boundary conditions on the transient response of FGM plate are depicted in Figs. 14-16, and it is observed that increasing the value of n, for all the boundary conditions (i.e., SSSS, CCCC, CSCS), increases the magnitude of deflection. Also, among all, CCCC type of boundary condition, results in least magnitude of deflection, i.e., clamped boundary condition has the maximum structural rigidity in terms of center deflection.

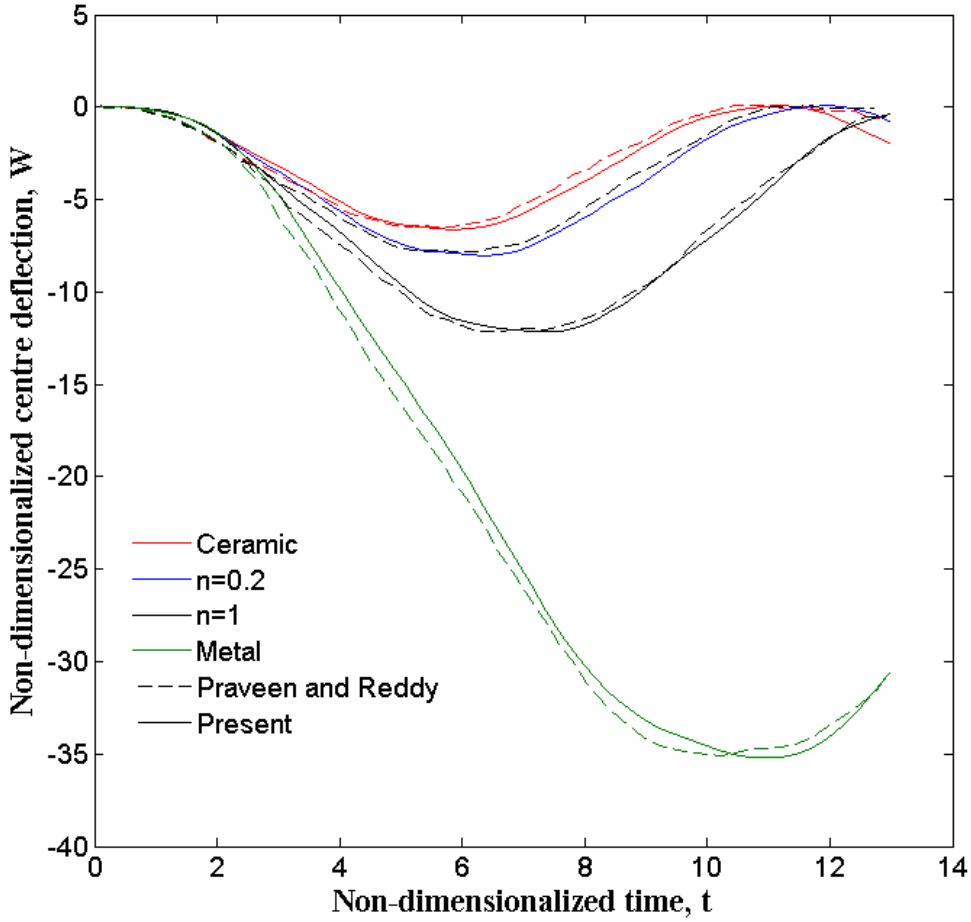

Fig. 13. The nonlinear transient response of simply supported square FGM (Aluminum-Alumina) plate under uniform lateral pressure loading.

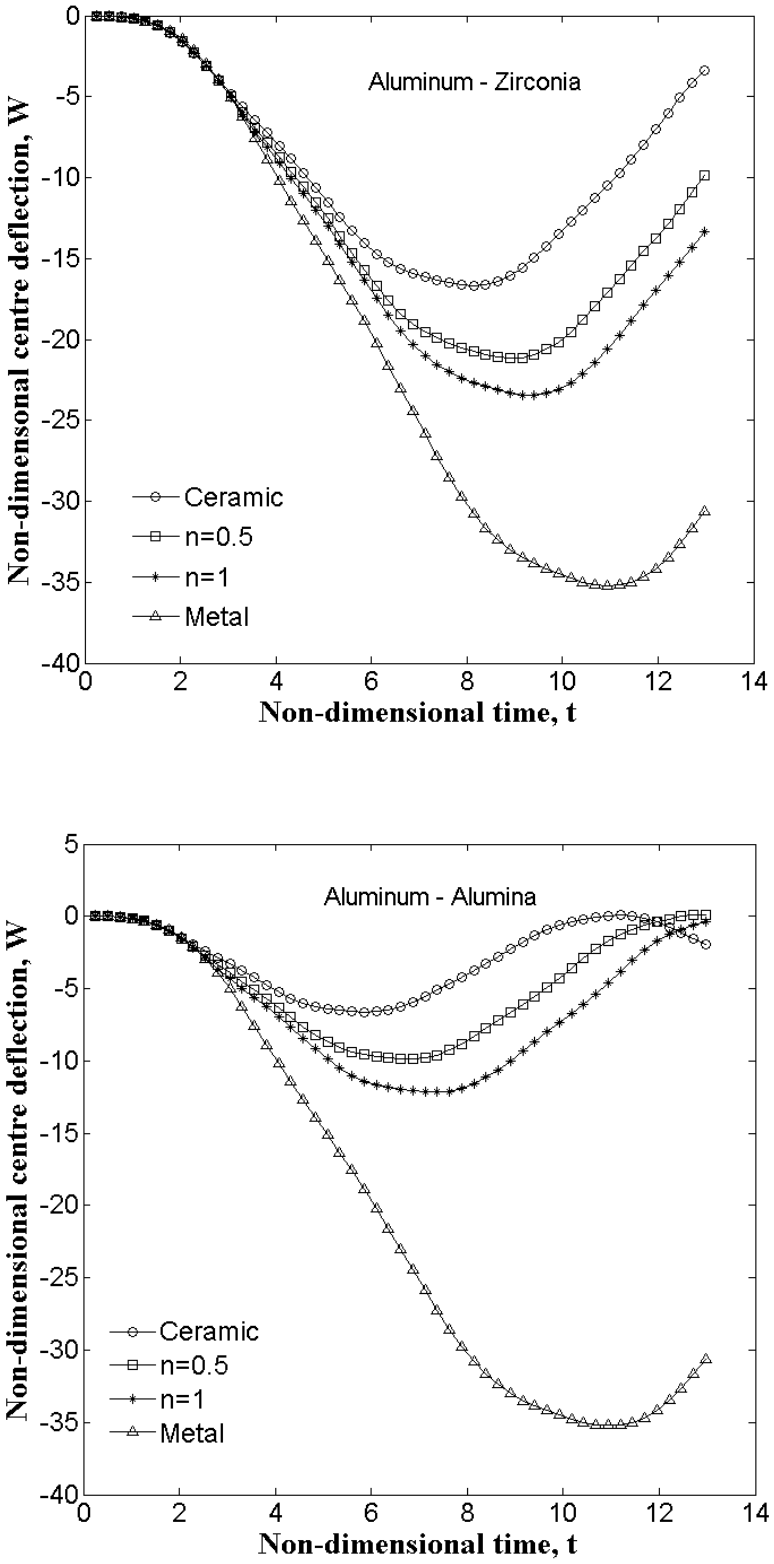

Fig. 14. The nonlinear transient response of SSSS square FGM plates under uniform lateral pressure loading.

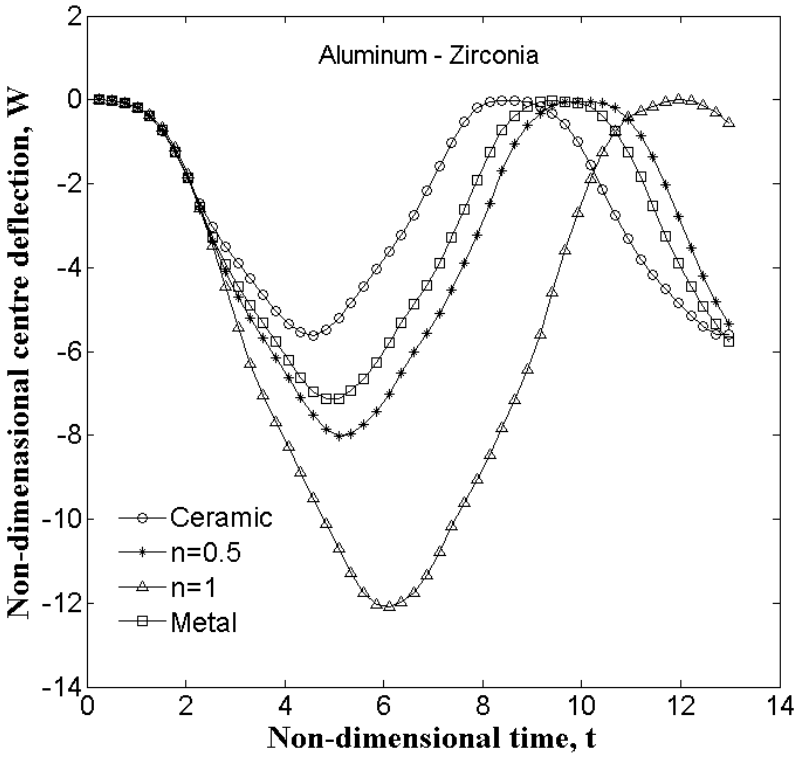

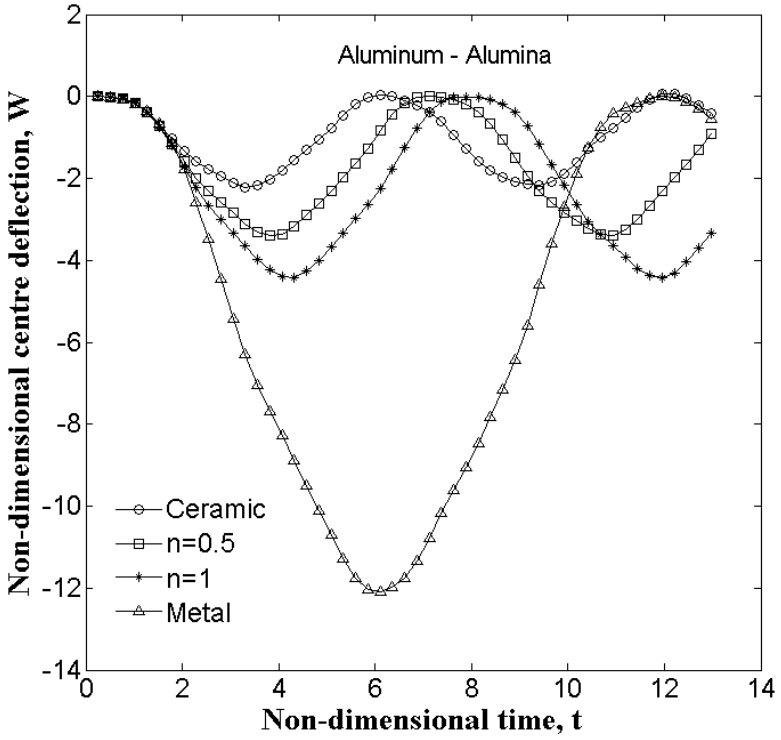

Fig. 15. The nonlinear transient response of CCCC square FGM plates under uniform lateral pressure loading.

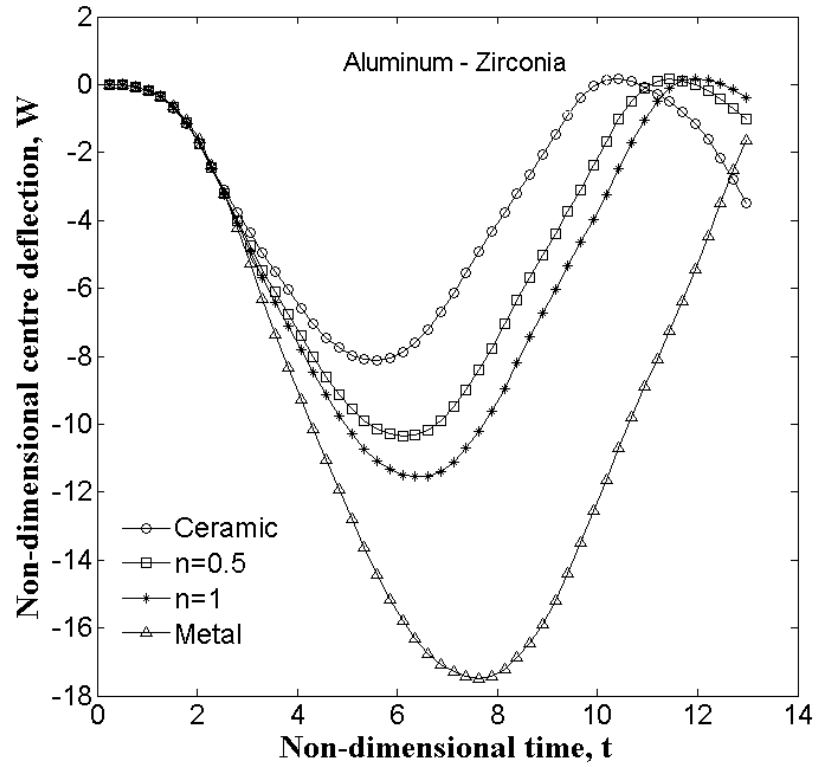

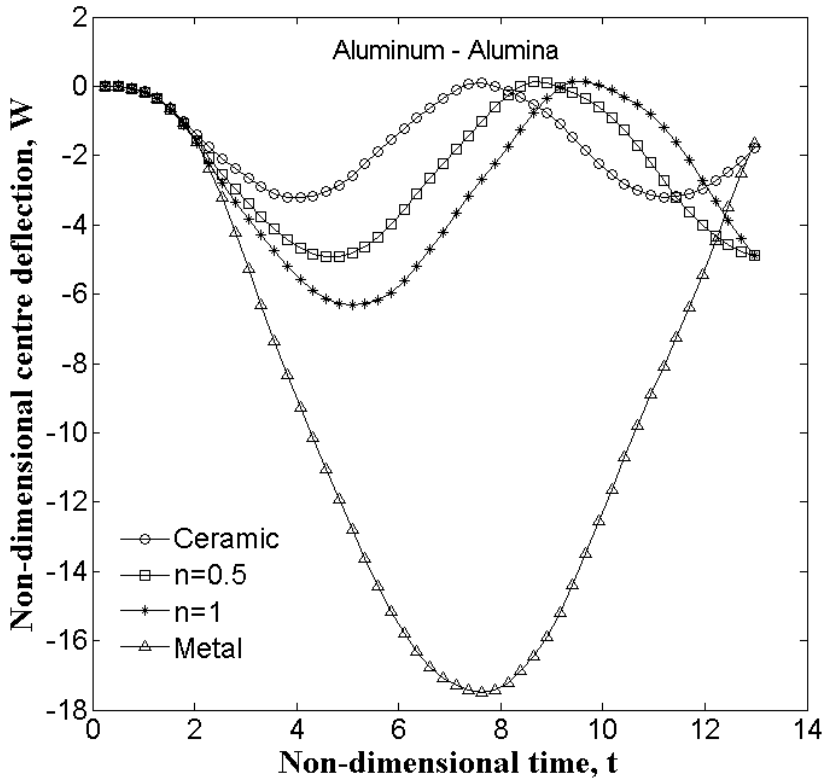

Fig. 16. The nonlinear transient response of CSCS square FGM plates under uniform lateral pressure loading.

4.4. Transient Response of Smart FGM plate Subjected to Thermo-Electro-Mechanical Load

By validating the code individually in Sections 4.2.2 and 4.3.1, for steady-state analysis of smart FGM plate under thermo-electro-mechanical load and for transient analysis of FGM plate under impact load, respectively, the procedure is proved valid even for the transient analysis of smart FGM under thermo-electro-mechanical load. Hence in this section, the analysis of an FGM plate bonded with piezoelectric layers on top and bottom surface is dealt with. The aluminum-zirconia combination for FGM layer and G-1195N for the piezoelectric layer are used as materials of construction, whose properties are same as given in Table 2.

In the parametric studies performed here, the thickness of piezoelectric layer h_p is taken as $h_p = 0.001\ m$, thickness of FGM layer as $h = 0.01\ m$ and the side of square plate as $a = 0.2\ m$. The temperatures prescribed on top and bottom surfaces are $300℃$ on and $20℃$, respectively. Value of power law index is taken as $n = 1$. The uniform lateral pressure of intensity $-11.5\ MPa$ is applied to the top surfaces of the plate structure, and the actuator voltage of $-100\ V$ is applied across the piezoelectric layers. An 8×8 uniform mesh of linear quadrilateral elements is used for the plate. Unless otherwise stated, these values of parameters are used consistently for all the studies performed in this section. For consistency, the time step size and range of time domain used is same as that used in previous section.

4.4.1 Effect of power law index

The temporal variations of central deflection of smart FGM plate are plotted in Figs. 17-19, for different values of power law index n, with different boundary conditions (i.e., SSSS, CCCC, CSCS).

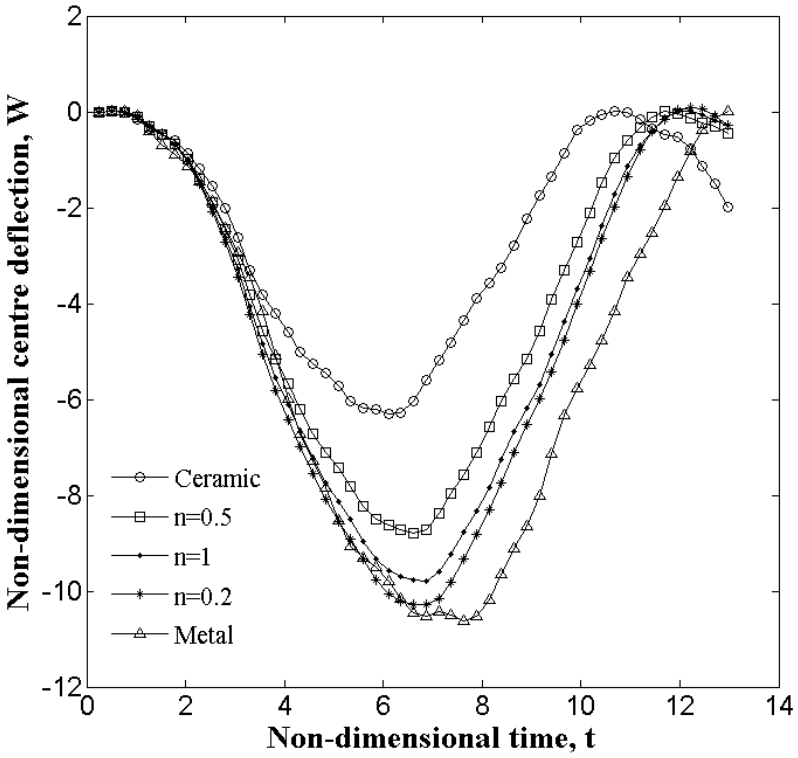

Fig. 17. Temporal variation of the nonlinear response of the square smart FGM plate with simply supported boundary conditions (SSSS).

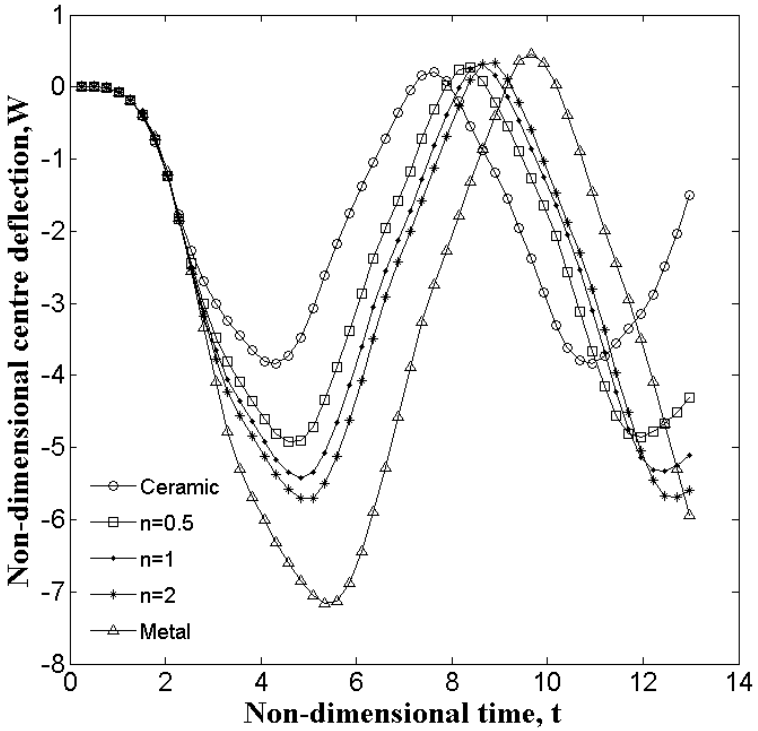

Fig. 18. Temporal variation of the nonlinear response of the square smart FGM plate with clamped boundary conditions (CCCC).

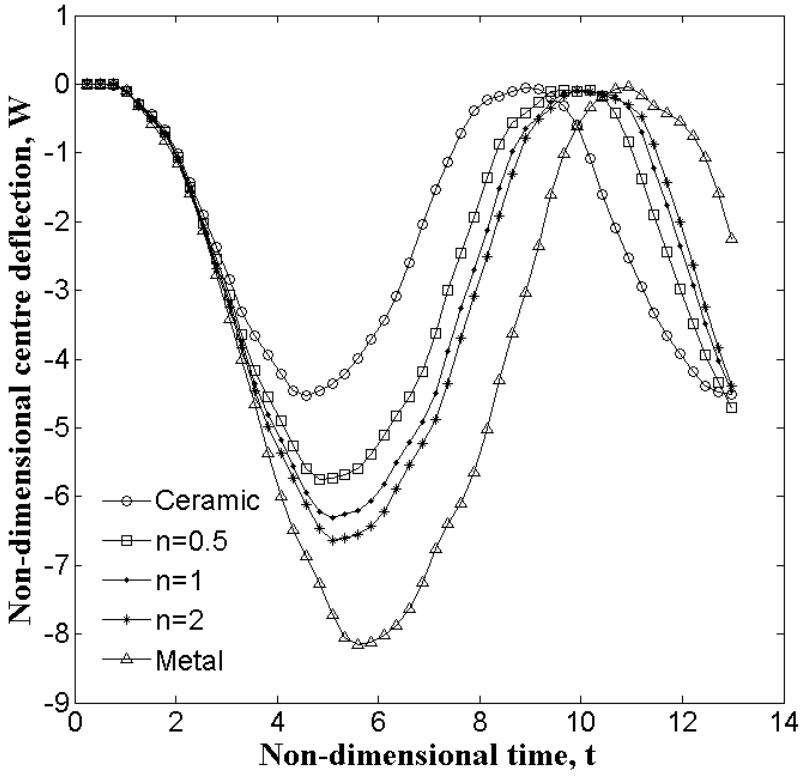

Fig. 19. Temporal variation of the nonlinear response of the square smart FGM plate with combined simply supported and clamped boundary conditions (CSCS).

As observed from Figs. 17-19, the increasing value of n makes the plate structure stiffer, however, not in proportion of n, i.e., deflection of a plate with $n = 0.5$ is not the average of the center deflections of plates with $n = 0$ and 1. The same observation was derived for all the boundary conditions.

4.4.2. Effect of slenderness ratio of the plate

The ratio of the span to the depth of an object is known as the slenderness ratio. In this section, the transient response of smart FGM plate is evaluated for the variation with slenderness ratio, for different boundary conditions (i.e., SSSS, CCCC, CSCS). The width of the plate a is kept constant, (i.e. $0.2\ m$) and the depth is varied to get different slenderness ratios.

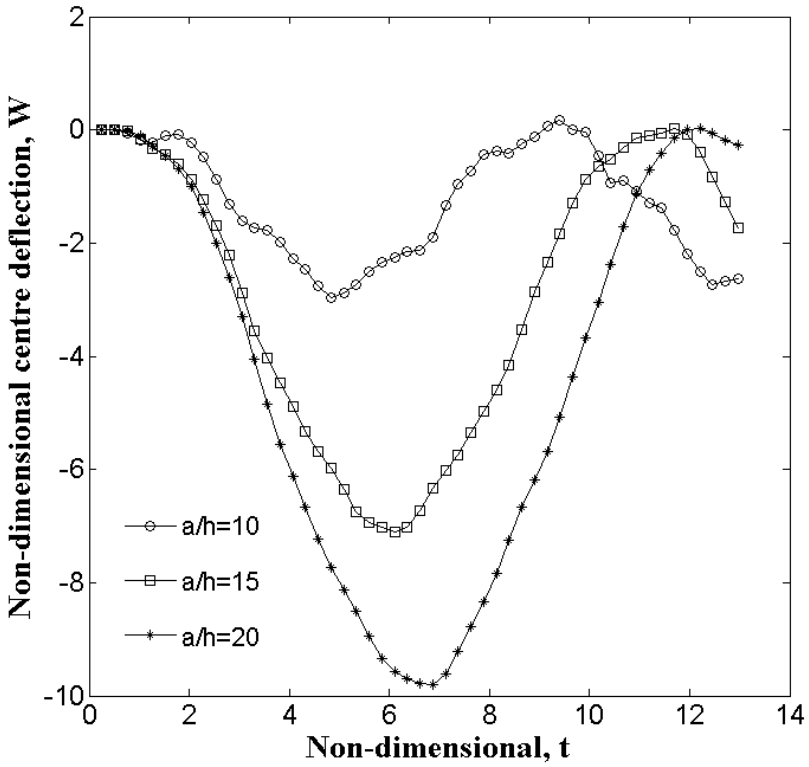

Fig. 20. Temporal variation of center deflection of smart FGM plate for different slenderness ratios, under simply supported (SSSS) boundary condition.

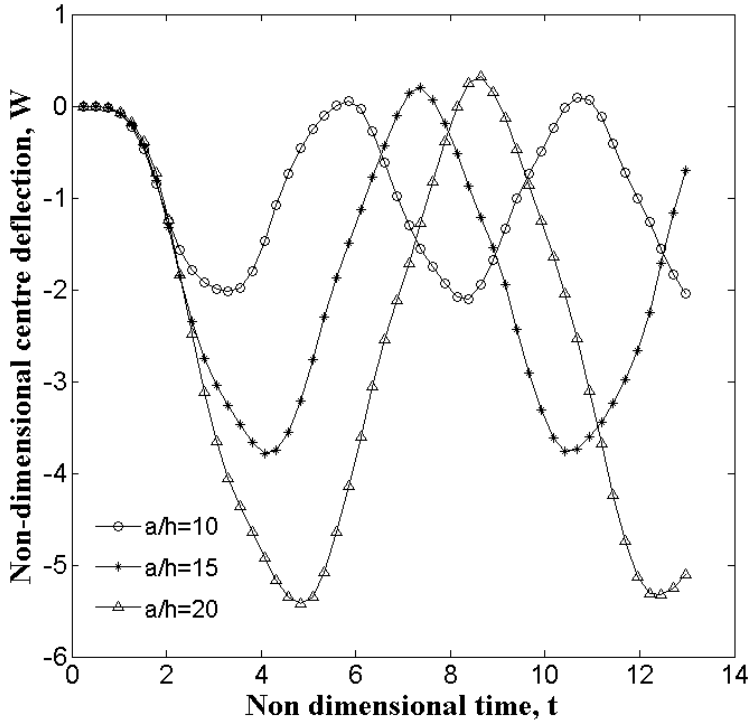

Fig. 21. Temporal variation of center deflection of smart FGM plate for different slenderness ratios, under clamped (CCCC) boundary condition.

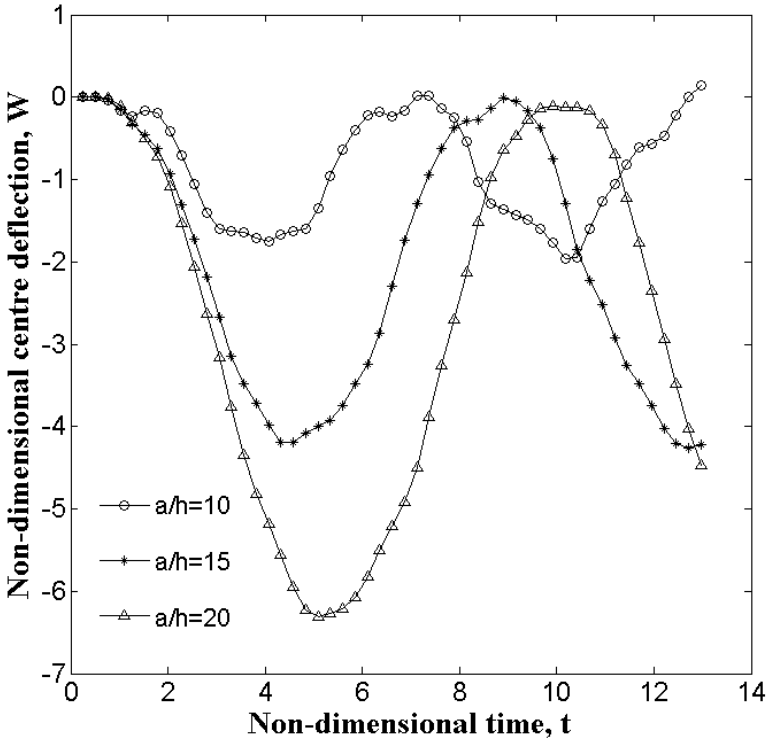

Fig. 22. Temporal variation of center deflection of smart FGM plate for different slenderness ratios under combined clamped and simply supported (CSCS) boundary conditions.

As observed from Figs. 20-22, as the slenderness ratio is increased the deflection in the plate increases, for all the boundary conditions. This is evident since the increasing slenderness ratio means thinner plate structure, which will have a lower value of stiffness resulting in high magnitudes of deflections.

4.4.3. Effect of ratio of FGM layer to piezoelectric layer thickness

The temporal variation of smart FGM plate with different h/h_p ratio for different boundary conditions is plotted, for different boundary conditions (i.e., SSSS, CCCC, CSCS) in Figs. 23-25. The thickness of FGM layer is kept constant, while the thickness of piezoelectric layers is varied to get different h/h_p ratios.

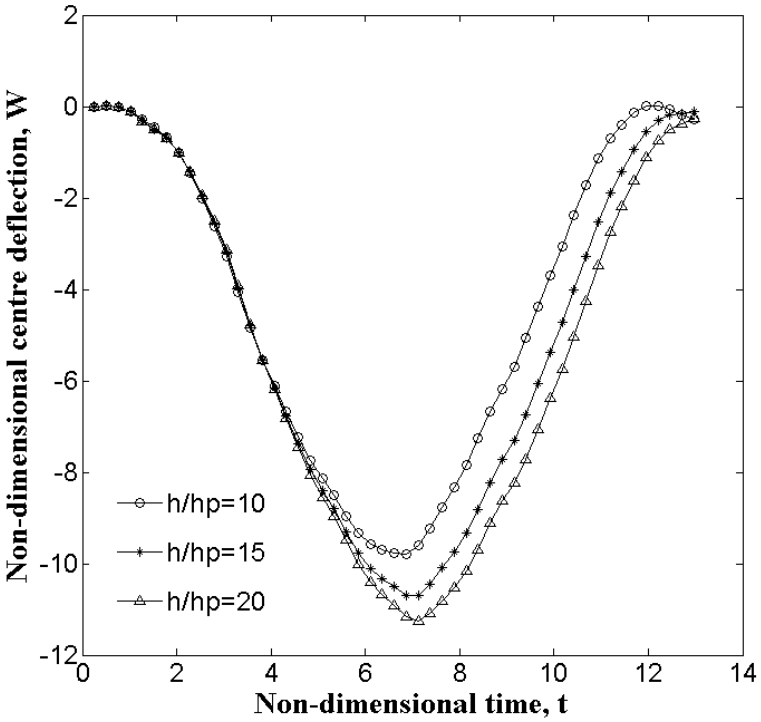

Fig. 23. Temporal variation of center deflection of smart FGM plate for different h/h_p ratios, under clamped (SSSS) boundary condition.

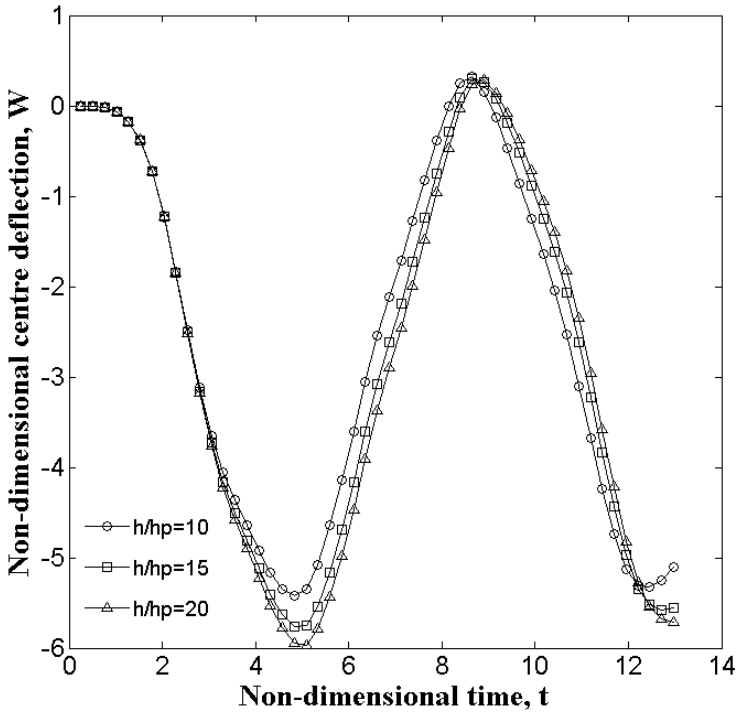

Fig. 24. Temporal variation of center deflection of smart FGM plate for different h/h_p ratios, under clamped (CCCC) boundary condition.

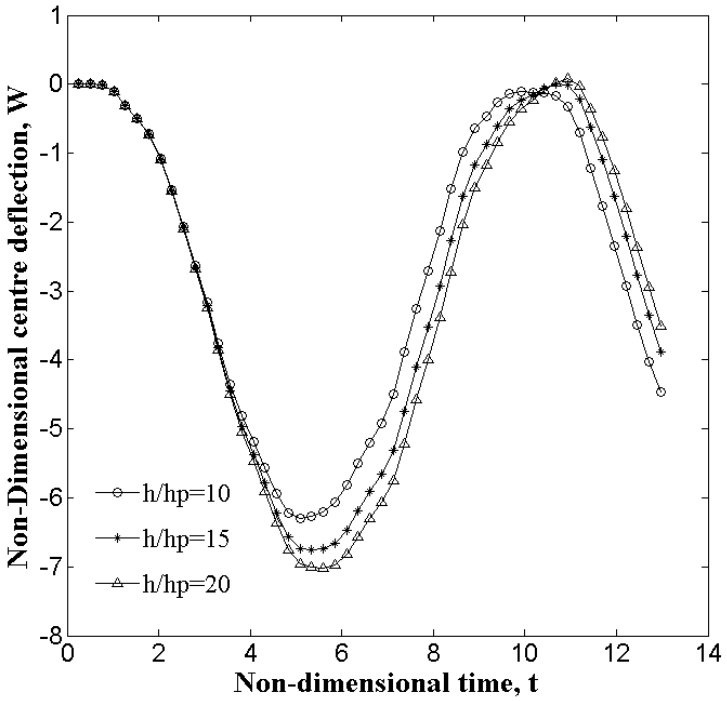

Fig. 25. Temporal variation of center deflection of smart FGM plate for different h/h_p ratios under combined clamped and simply supported (CSCS) boundary conditions.

As observed from Figs. 23-25, it can be said that the actuation effect in the plate structure can be increased by increasing the thickness of the piezoelectric layer, in comparison to the thickness of FGM layer. Hence for a particular value of applied actuator voltage, deflection can be controlled more efficiently, by decreasing h/h_p ratio. The same observation was found to be consistent for all the boundary conditions.

Effect of applied actuator voltage

The voltage applied on piezoelectric actuator layers produces a deflection in the plate and in response to the mechanical strain, the plate produces an electric pulse, these phenomena are known as direct piezoelectric effect and reverse piezoelectric effect respectively. The behavior of piezoelectric FGM plate under direct piezoelectric effect is studied in this section; which is used in controlling the temporal variations of center deflection of the plate. Three values of voltage are applied on a smart FGM plate, with other parameters kept constant. Power law index is taken as 1, and a/h ratio is 20.

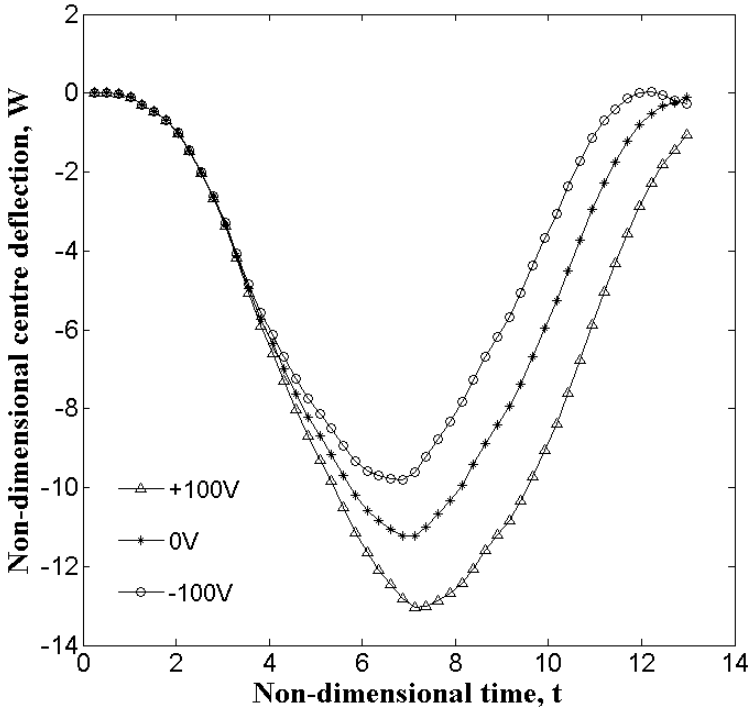

Fig. 26. Temporal variation of center deflection of smart FGM plate for different values of applied actuator voltage under simply supported (SSSS) boundary conditions.

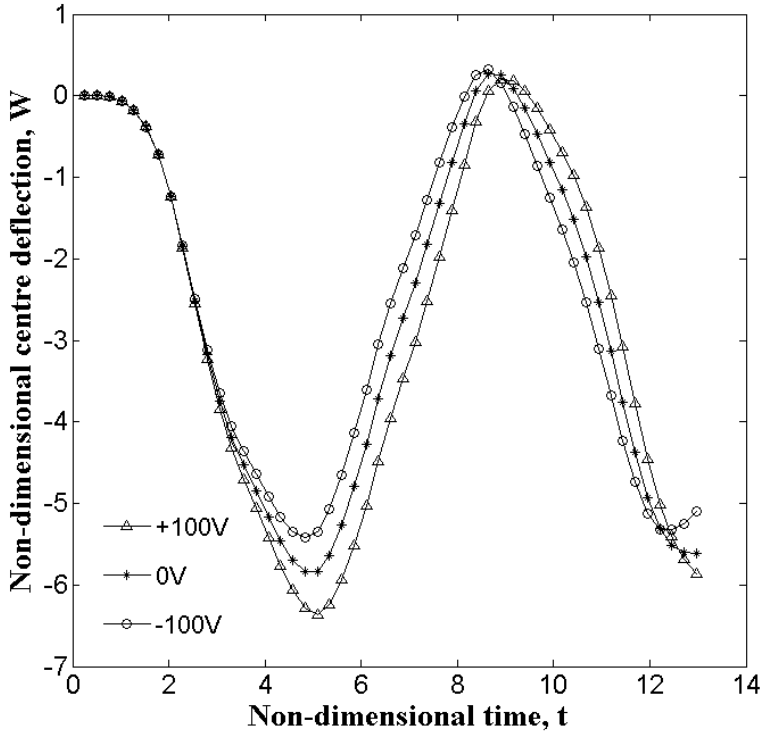

Fig. 27. Temporal variation of center deflection of smart FGM plate for different values of applied actuator voltage under clamped (CCCC) boundary conditions.

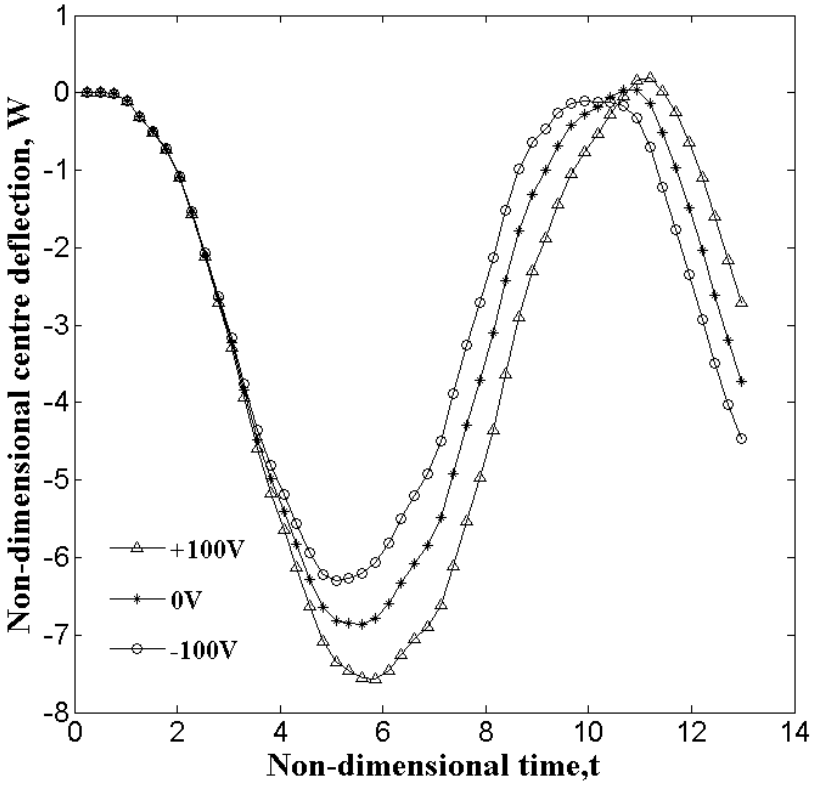

Fig. 28. Temporal variation of center deflection of smart FGM plate for different values of applied actuator voltage under combined clamped and simply supported (CSCS) boundary conditions.

To investigate the effect of applied actuator voltage on the nonlinear electro-thermo-mechanical, transient response, the temporal variations of center deflection of the plate under $+100V, 0V \; and \; -100V$, are plotted in Figs. 26-28, for different boundary conditions (i.e., SSSS, CCCC, CSCS). It is observed that, for all the boundary conditions, the amplitude of vibration in the plate due to impact load is increased when a positive voltage is applied and decrease under a negative voltage, as compared to the amplitude under $O\,V$, which denotes the ground state. Also, the effect of voltage on temporal evolution of deflection is negligible for initial time steps and becomes significant only after a few time steps.

Chapter 5

CONCLUSION AND FUTURE SCOPE

5.1. Conclusion

The geometrically nonlinear responses of FGM and smart FGM plates were studied, under different types of boundary and loading conditions. Mindlin's first-order shear deformation plate theory was used to develop the finite element model. An uncoupled ESL model is used to account for the electromechanical effect. In all the analyses zirconia-aluminum based FGM and G-1195N piezoelectric materials were used. Based on these analyses following key conclusion are derived:

- The applied actuator voltage controls the nonlinear transient response of plate significantly. A positive voltage increases the negative deflection of the plate, whereas, by applying a negative voltage, negative deflection decreases as compared to the deflection when no voltage is applied, i.e. grounded condition. This characteristic of the piezoelectric material can be utilized in vibration suppressing and monitoring devices.
- The actuation effect of the piezoelectric layer is prominent at the plate with thinner FGM layers. When the thickness of the FGM layer is increased in comparison to that of the piezoelectric layer, the controlling or the actuation effect decreases significantly.
- The response of plate for three different values of voltages, $+100\ V, 0\ V, and\ -100V$ does not differ significantly just after the application of the load. This means that the actuation effect of piezoelectric layers is not very effective for a few initial time steps. But as the time progresses the actuation effects becomes prominent rapidly. From this behavior, it can be concluded that the role piezoelectric actuation effect takes time to appear. Hence, the response time of piezoelectric layers is critical and should be taken into account while designing an actual system.

5.2. Future Scope

In the analyses presented, an uncoupled ESL model of the smart FGM plate was used. Based on the validation study results can be said to be reasonably accurate, for practical applications, where required level of accuracy is much higher, a coupled model should be used in developing the formulation. Also, this thesis is focused only on direct piezoelectric effects which are useful in actuation applications. The reverse piezoelectric effect should also be studied against all the parameters and variations, which is helpful in monitoring the real-time behavior of the structure during application.

REFERENCES

[1] B. Kieback, A. Neubrand, and H. Riedel, “Processing techniques for functionally graded materials ଼,” vol. 362, pp. 81–105, 2003.

[2] C. A. I. Board, “Columbia Accident Investigation Board,” 2003.

[3] M. Koizumi, “FGM activities in Japan,” *Compos. Part B Eng.*, vol. 28, no. 1–2, pp. 1–4, 1997.

[4] R. M. Mahamood, E. T. A. Member, M. Shukla, and S. Pityana, “Functionally Graded Material : An Overview,” *World Congr. Eng.*, vol. III, pp. 2–6, 2012.

[5] R. M. Mahamood and E. T. Akinlabi, “Functionally Graded Materials,” 2017.

[6] J.N. Reddy, “Mechanics of laminated composite plates and shells: theory and analysis.” p. 840, 2003.

[7] Y. Miyamoto, W. A. Kaysser, B. H. Rabin, A. Kawasaki, and R. G. Ford, *Functionally graded materials: design, processing and applications*. 1999.

[8] V. Giurgiutiu, “Actuators and Smart Structures,” *Encycl. Vib.*, pp. 58–81, 2001.

[9] M. Shen and M. B. Bever, “Gradients in polymeric materials,” *J. Mater. Sci.*, vol. 7, no. 7, pp. 741–746, 1972.

[10] M. B. Bever and P. E. Duwez, “Gradients in composite materials,” *Mater. Sci. Eng.*, vol. 10, pp. 1–8, 1972.

[11] H. U. Akay, “Dynamic large deflection analysis of plates using mixed finite elements,” no. June, 1979.

[12] J. N. Reddy, “Geometrically nonlinear transient analysis of laminated composite plates,” *AIAA J.*, vol. 21, no. 4, pp. 621–629, 1983.

[13] J. N. Reddy, “Dynamic (transient) analysis of layered anisotropic composite-material plates,” *Int. J. Numer. Methods Eng.*, vol. 19, no. 2, pp. 237–255, 1983.

[14] G. N. Praveen and J. N. Reddy, “Nonlinear Transient Thermoelastic Analysis of Functionally Graded Ceramic-metal Plates,” *Int. J. Solids Struct.*, vol. 35, no. 33, pp. 4457–4476, 1998.

[15] J. N. Reddy & C. D. Chin, “Thermomechanical Analysis of Functionally Graded Cylinders and Plates,” *J. Therm. Stress.*, vol. 21, no. 6, pp. 593–626, 1998.

[16] J. N. Reddy, “Analysis of functionally graded plates,” *Int. J. Numer. METHODS Eng. Int. J. Numer. Meth. Engng*, vol. 47, no. June 1999, pp. 663–684, 2000.

[17] J. Woo and S. a. Meguid, “Nonlinear analysis of functionally graded plates and shallow shells,” *Int. J. Solids Struct.*, vol. 38, no. 42–43, pp. 7409–7421, 2001.

[18] J. YANG and H.-S. SHEN, “Vibration Characteristics and Transient Response of Shear-Deformable Functionally Graded Plates in Thermal Environments,” *J. Sound Vib.*, vol. 255, no. 3, pp. 579–602, 2002.

[19] J. Yang and H.-S. Shen, “Non-linear analysis of functionally graded plates under transverse and in-plane loads,” *Int. J. Non. Linear. Mech.*, vol. 38, no. 4, pp. 467–482, 2003.

[20] L. F. Qian, R. C. Batra, and L. M. Chen, “Static and dynamic deformations of

thick functionally graded elastic plates by using higher-order shear and normal deformable plate theory and meshless local Petrov – Galerkin method," vol. 35, pp. 685–697, 2004.

[21] H. S. Shen, "Nonlinear bending response of functionally graded plates subjected to transverse loads and in thermal environments," *Int. J. Mech. Sci.*, vol. 44, no. 3, pp. 561–584, 2002.

[22] L. F. Qian and R. C. Batra, "Transient thermoelastic deformations of a thick functionally graded plate," *J. Therm. Stress.*, vol. 27, no. 8, pp. 705–740, 2004.

[23] P. Malekzadeh and S. M. Monajjemzadeh, "Dynamic response of functionally graded plates in thermal environment under moving load," *Compos. Part B Eng.*, vol. 45, no. 1, pp. 1521–1533, 2013.

[24] H. Bellifa, K. H. Benrahou, L. Hadji, M. S. A. Houari, and A. Tounsi, "Bending and free vibration analysis of functionally graded plates using a simple shear deformation theory and the concept the neutral surface position," *J. Brazilian Soc. Mech. Sci. Eng.*, vol. 38, no. 1, pp. 265–275, 2016.

[25] Y. Z. Wang, D. Liu, Q. Wang, and J. Z. Zhou, "Asymptotic analysis of thermoelastic response in functionally graded thin plate subjected to a transient thermal shock," *Compos. Struct.*, vol. 139, pp. 233–242, 2016.

[26] H. S. Tzou and M. Cadre, "Theoretical Coupled for Analysis Distributed of Multi-Layered Controls Thin With Piezoelectric Vibration," vol. 132, pp. 433–450, 1989.

[27] K. D. Jonnalagadda, G. E. Blandford, and T. R. Tauchert, "Piezothermoelastic composite plate analysis using first-order shear deformation theory," *Comput. Struct.*, vol. 51, no. 1, pp. 79–89, 1994.

[28] X. H. Wu, C. Chen, Y. P. Shen, and X. G. Tian, "A high order theory for functionally graded piezoelectric shells," *Int. J. Solids Struct.*, vol. 39, no. 20, pp. 5325–5344, 2002.

[29] H. S. Shen, "Thermal postbuckling of shear-deformable laminated plates with piezoelectric actuators," *Compos. Sci. Technol.*, vol. 61, no. 13, pp. 1931–1943, 2001.

[30] M. Ishihara and N. Noda, "PIEZOTHERMOELASTIC ANALYSIS OF A CROSS-PLY," no. June 1999, pp. 3–5, 2000.

[31] A. Benjeddou, "Advances in piezoelectric finite element modeling of adaptive structural elements: a survey," *Comput. Struct.*, vol. 76, no. 1, pp. 347–363, 2000.

[32] J. N. Reddy, "On laminated composite plates with integrated sensors and actuators," *Eng. Struct.*, vol. 21, no. 7, pp. 568–593, 1999.

[33] H.-J. Lee and D. A. Saravanos, "Generalized finite element formulation for smart multilayered thermal piezoelectric composite plates," *Int. J. Solids Struct.*, vol. 34, no. 26, pp. 3355–3371, 1997.

[34] S. Kapuria, G. P. Dube, P. C. Dumir, and S. Sengupta, "Levy-type piezothermoelastic solution for hybrid plate by using first-order shear deformation theory," *Compos. Part B Eng.*, vol. 28, no. 5–6, pp. 535–546, 1997.

[35] K. Y. Lam and T. Y. Ng, "Active control of composite plates with integrated piezoelectric sensors and actuators under various dynamic loading conditions,"

Smart Mater. Struct., vol. 8, no. 2, p. 223, 1999.

[36] Y. Ootao and Y. Tanigawa, "Three-dimensional transient piezothermoelasticity in functionally graded rectangular plate bonded to a piezoelectric plate," *Int. J. Solids Struct.*, vol. 37, no. 32, pp. 4377–4401, 2000.

[37] K. M. Liew, X. Q. He, T. Y. Ng, and S. Sivashanker, "Active control of FGM plates subjected to a temperature gradient: Modelling via finite element method based on FSDT," *Int. J. Numer. Methods Eng.*, vol. 52, no. 11, pp. 1253–1271, 2001.

[38] T. Y. Ng, X. Q. He, and K. M. Liew, "Finite element modeling of active control of functionally graded shells in frequency domain via piezoelectric sensors and actuators," *Comput. Mech.*, vol. 28, no. 1, pp. 1–9, 2002.

[39] F. Ebrahimi and A. Rastgoo, "Free vibration analysis of smart annular FGM plates integrated with piezoelectric layers," *Smart Mater. Struct.*, vol. 17, no. 1, p. 15044, 2008.

[40] S. Kapuria, M. Bhattacharyya, and A. N. Kumar, "Bending and free vibration response of layered functionally graded beams: A theoretical model and its experimental validation," *Compos. Struct.*, vol. 82, no. 3, pp. 390–402, 2008.

[41] J. Yang, S. Kitipornchai, and K. M. Liew, "Non-linear analysis of the thermo-electro-mechanical behaviour of shear deformable FGM plates with piezoelectric actuators," *Int. J. Numer. Methods Eng.*, vol. 59, no. 12, pp. 1605–1632, 2004.

[42] J. N. Reddy and Z.-Q. Cheng, "Three-Dimensional Solutions of Smart Functionally Graded Plates," *J. Appl. Mech.*, vol. 68, no. 2, p. 234, 2001.

[43] J. Zhang and X. Zhao, "Thermal Shock Buckling of a Functionally Graded Circular Plate," in *ASME 2016 International Mechanical Engineering Congress and Exposition*, 2016, p. V001T03A011-V001T03A011.

[44] N. D. Duc, T. Q. Quan, and V. D. Luat, "Nonlinear dynamic analysis and vibration of shear deformable piezoelectric FGM double curved shallow shells under damping-thermo-electro-mechanical loads," *Compos. Struct.*, vol. 125, pp. 29–40, 2015.

[45] S. Committee, I. Ultrasonics, and F. C. Society, "An American National Standard IEEE Standard on Piezoelectricity," 1988.

[46] W. Lanhe, "Thermal buckling of a simply supported moderately thick rectangular FGM plate," *Compos. Struct.*, vol. 64, no. 2, pp. 211–218, 2004.

[47] J. N. Reddy, *Energy principles and variational methods in applied mechanics*. John Wiley & Sons, 2017.

[48] J. N. Reddy, *An introduction to nonlinear finite element analysis*, vol. 1, no. 2. 2004.

[49] K.-J. Bathe, *Finite element procedures*. Klaus-Jurgen Bathe, 2006.

[50] K. M. Mathisen, "(PPT) Solution Methods for Nonlinear Finite Element Analysis (NFEA)," *Lecture*, vol. 11, p. 39, 2012.

[51] J. W. LEECH, "Stability of Finite-Difference Equation for the Transient Response of a Flat Plate," *AIAA J.*, vol. 3, no. 9, pp. 1772–1773, Sep. 1965.

Nonlinear Transient Analysis of Piezoelectric FGM Plate Under Electro-Thermo-Mechanical Loading

ORIGINALITY REPORT

%19	%6	%18	%
SIMILARITY INDEX	INTERNET SOURCES	PUBLICATIONS	STUDENT PAPERS

PRIMARY SOURCES

1	Ming-Jun Lai. "Bivariate spline method for numerical solution of steady state Navier–Stokes equations over polygons in stream function formulation", Numerical Methods for Partial Differential Equations, 03/2000 Publication	%1
2	Y. X. Hao. "Nonlinear Dynamic Response of Functionally Graded Rectangular Plates under Different Internal Resonances", Mathematical Problems in Engineering, 2010 Publication	%1
3	www.esm.vt.edu Internet Source	<%1
4	Fakhari, V.. "Nonlinear free and forced vibration behavior of functionally graded plate with piezoelectric layers in thermal environment", Composite Structures, 201108 Publication	<%1
5	J. Yang. "Non-linear analysis of the thermo-	